Pharmacological targeting of Sphingosine-1-phosphate Lyase (SGPL1) modulates (glyco)sphingolipid metabolism and results therapeutically effective in experimental models of Huntington's disease

Giuseppe Pepe[1], Luca Capocci[1], Federico Marracino[1], Natalia Realini[2], Aynur Sönmez[3,11], Paola Lenzi[4], Katiuscia Martinello[1], Tiziana F Bovier[5,6], Terry Jo Bichell[7], Pamela Scarselli[1], Clotilde Di Cicco[1], Aaron Bowman[8], Filomena A Digilio[5], Sergio Fucile[1,9], Francesco Fornai[1,4], Andrea Armirotti[2], Rosanna Parlato[10], Alba Di Pardo[1] and Vittorio Maglione[1,12,*]

[1]IRCCS Neuromed; Pozzilli (IS), 86077, Italy

[2]Analytical Chemistry Lab, Fondazione Istituto Italiano di Tecnologia, Via Morego 30, 16163 Genoa, Italy

[3] Institute of Applied Physiology, Ulm University, Ulm, Germany.

[4]Department of Translational Research and New Technologies in Medicine and Surgery, University of Pisa, Via Roma 55, 56126 Pisa, Italy.

[5]Research Institute on Terrestrial Ecosystems (IRET), UOS Naples-CNR,
Via Pietro Castellino 111, 80131 Naples, Italy

[6] Department of Pediatrics Columbia University Vagelos College of Physicians and Surgeons, New York, NY, USA; Center for Host–Pathogen Interaction, Columbia
University Vagelos College of Physicians and Surgeons, New York, NY, USA.

[7]Vanderbilt Brain Institute, Vanderbilt University, United States

[8]School of Health Sciences, Purdue University, West Lafayette, IN, United States of America.

[9]Department of Physiology and Pharmacology, Istituto Pasteur-Fondazione Cenci Bolognetti, University of Rome Sapienza, Rome, Italy.

[10]Division for Neurodegenerative Diseases, Department of Neurology, Mannheim Center for Translational Neuroscience, Medical Faculty Mannheim, Heidelberg University, Mannheim, Germany; Institute of Applied Physiology, Ulm University, Ulm, Germany

[11]Present address: RNA Molecular Biology, Fonds de la Recherche Scientifique (F.R.S./FNRS), Université Libre de Bruxelles (ULB), Biopark campus, Gosselies, Belgium.

[12]Lead contact

[*]Correspondence: vittorio.maglione@neuromed.it (V.M.)

Summary

Huntington's disease (HD) is the most common neurodegenerative disorder with no effective cure currently available. Over the past few years our research has shown that alterations in sphingolipid metabolism represent a critical determinant in the pathogenesis of the disease. In particular, aberrant metabolism of sphingosine-1-phosphate (S1P) has been reported in multiple disease settings including human post-mortem brains from HD patients.

In this study, we investigated any potential therapeutic effect of the inhibition of S1P degradative enzyme SGPL1.

Our results demonstrated that chronic administration of the THI inhibitor mitigated motor dysfunctions in both mouse and fly models of HD. The compound evoked the activation of pro-survival pathways, normalized levels of BDNF, preserved white matter integrity and stimulated synaptic functions in HD mice.

Under metabolic point of view THI restored normal levels of hexosylceramides and stimulates autophagic and lysosomal machinery, facilitating the reduction of nuclear inclusions of both wt- and mutant protein.

Keywords: Htt, THI, Glucosylceramide, Neurodegeneration, Neuroprotection, Therapeutics

Introduction

Huntington's disease (HD) is the most common dominantly inherited neurodegenerative disorder characterized by the progressive striatal and cortical degeneration and associated motor, cognitive and behavioral disturbances (Tabrizi et al., 2020). The disease-causing mutation is a polyglutamine (polyQ) stretch within the N-terminal of huntingtin (Htt), a ubiquitous expressed and brain-enriched protein which plays a role in multiple cellular pathways (Saudou and Humbert, 2016).

When mutated, Htt exerts a variety of undesirable toxic effects in both neuronal and non-neuronal cells (Chuang and Demontis, 2021; Tabrizi et al., 2020; Wilton and Stevens, 2020) and, it interferes with cellular metabolism at multiple levels (Bichell et al., 2017; Sbodio et al., 2018; Singh and Agrawal, 2021).

Among all the metabolic dysfunctions associated with HD, alterations in the metabolism of some glycosphingolipid species (gangliosides) seem to contribute to its pathogenesis (Denny et al., 2010; Desplats et al., 2007; Maglione et al., 2010; Di Pardo et al., 2016). Decreased gene expression of specific ganglioside-metabolizing enzymes, has been described in multiple HD pre-clinical models and in HD patients (Hunter et al., 2021; Maglione et al., 2010; Di Pardo et al., 2016).

Number of evidence indicates that expression of enzymes involved in the metabolism of other sphingolipids is also aberrant in HD and, it may likely represent a potential therapeutic target (Moruno-Manchon et al., 2017; Di Pardo and Maglione, 2018; Di Pardo et al., 2018, 2019; Pirhaji et al., 2017). In particular, sphingosine -1- phosphate (S1P) metabolism has been described to be dysfunctional in multiple HD experimental models as well as in HD human post-mortem brain tissues (Di Pardo et al., 2017a, 2017b; Pirhaji et al., 2016, 2017).

S1P is one of the most potent signalling lipids, that governs essential physiological processes underlying neuronal functions and overall cellular homeostasis and viability (Ayub et al., 2021; Van Echten-Deckert et al., 2014; Grassi et al., 2019).

Metabolism of S1P is a quite complex biological process in which a number of different highly specialized enzymes is involved and a fine balance between synthesis and degradation is normally required for cellular homeostasis and functions. S1P is typically synthesized by sphingosine kinase-1 and -2 (SPHK1 and 2), and commonly irreversible degraded by sphingosine-1-phosphate lyase (SGPL1) (Maceyka et al., 2012).

Reduced levels of SPHK1 and concomitant elevation of SGPL1, has been reported in different HD models as well as in human post-mortem brains from HD patients (Di Pardo et al., 2017a). This imbalance may plausibly underlie the decremented bioavailability of S1P (Di Pardo et al., 2017a).

The degradative enzyme SGPL1 represents a key regulator in the maintenance of balanced S1P levels and other sphingolipid intermediates that influence various aspects of cell growth, proliferation and cell death (Serra and Saba, 2010).

The role of SGPL1 in the nervous system is still debated and at times controversial (Alam et al., 2020; Blaho, 2020; Hagen et al., 2009, 2011). While specific inactivation of SGPL1, in neurons, induces S1P accumulation, altering presynaptic functions (Mitroi et al., 2016) and autophagic flux (Mitroi et al., 2017), full body partial ablation of *Sgpl1* gene does not lead to any accumulation of S1P in brain tissues and results beneficial in a mouse model of experimental autoimmune encephalomyelitis (Billich et al., 2013).

Inhibition of SGPL1, by the caramel color 2-acetyl-5-tetrahydroxybutyl imidazole (THI) (Vollmuth, 2018), reduced cell apoptosis in different *in vitro* HD models (Moruno Manchon et al., 2015; Di Pardo et al., 2017a) and suppressed dystrophic muscle degeneration in experimental models of Duchenne muscle dystrophy (Nguyen-Tran et al., 2014).

In the present study, we reported the therapeutic potential of THI in two different *in vivo* experimental model of HD.

THI exerted normalized levels of BDNF with associated neuroprotective effect, preserved myelin integrity and stimulated synaptic functions in HD mice. Also, it normalized levels of glycosphingolipid (hexosylceramides), activated autophagy and reduced Htt accumulation in the brain of HD mice.

Our findings further support the concept that the alteration of (glyco)sphingolipid pathways may contribute to the pathogenesis of the disease and that it may be pharmacologically targeted for the development of potential alternative therapeutic approaches for HD.

Results

Treatment with THI mitigates motor deficit and evokes the activation of pro-survival pathways in R6/2 mice

In order to test the hypothesis that inhibition of SGPL1 might be beneficial in *in vivo* models of HD, early manifest R6/2 mice (6-week old) and aged-matched wild-type (WT) littermates were daily intraperitoneally (i.p.)- injected with either 0.1 mg/kg THI, the lowest concentration reported to be safe *in vivo* (GOBIN and PHILLIPS, 1991), or vehicle, and motor function was analyzed.

THI-treated HD mice did not exhibit the characteristic clasping behavior (Figure 1A-B) and performed significantly better than vehicle-treated controls during the whole period of the treatment as assessed by Rotarod and Horizontal Ladder Task (Fig. 1C-D). Also, both brain and body weight

loss were attenuated by administration of the compound (Fig. 1E-F). No evidence of adverse events was observed in WT animals.

Next, we explored any potential neuroprotective effect of THI in R6/2 mouse brain. Administration of the compound was associated with increased phosphorylation of the pro-survival kinase AKT (Fig. 1G) and increased protein expression of striatal dopamine- and cAMP-regulated protein 32 (DARPP-32) (Fig. 1H), a specific marker of medium spiny neurons (Matamales et al., 2009), whose downregulation classically correlates with neurodegeneration in HD (Ehrlich, 2012). Importantly, THI administration preserved normal levels of brain derived neurotrophic factor (BDNF) in both striatum and cortex of R6/2 mice (Figure 1I-L).

THI treatment preservers white-matter integrity and ameliorates synaptic activity in HD cortical pyramidal neurons

Alterations in the Corpus Callosum (CC) and white-matter integrity have been reported , early in the disease in both HD animal models and human patients (Dumas et al., 2012; Estevez-Fraga et al., 2020; Gatto et al., 2021; Di Paola et al., 2014; Di Pardo et al., 2016).

Semi-quantitative analysis of anatomical structure of CC revealed that chronic infusion of the compound prevented the classical reduction of its thickness (Di Pardo et al., 2014) in R6/2 mice (Fig. 2A-B).

Changes in the CC of THI-treated R6/2 mice were associated with preservation of normal levels of the myelin markers, myelin basic protein (MBP) and myelin–associated glycoprotein (MAG) (Fig. 2C-D).

The beneficial effect of the treatment was confirmed by electron microscopy, which revealed the presence of giant axons with abnormal myelin sheaths and negligible axoplasm electro density in R6/2 mice (Fig. 2E). Treatment with THI increased myelin thickness (Fig. 2F) and reduced maximum, minimum and medium axonal diameter in HD (Fig. 2G-I).

Further proofs of the ability of the compound to preserve axonal homeostasis and neuronal functions in HD mice came from both molecular and electrophysiological studies.

Treatment with THI preserved normal levels of post-synaptic density-95 protein (PSD-95) in both striatum and cortex of HD mice (Fig. 2L-M).

PSD-95, a major constituent of glutamatergic excitatory synapses, is specifically enriched at the postsynaptic density (PSD) and can regulate the Alpha-Amino-3-Hydroxy-5-Methyl-4-Isoxazole Propionic Acid (AMPA) and the N-Methyl-D-Aspartic acid (NMDA) receptors expression and activity in spines (Kim and Sheng, 2004; Won et al., 2016).

In light of that, we decided to record spontaneous excitatory post-synaptic currents (EPSCs) from L5 pyramidal neurons in temporal slices of WT and R6/2 mice.
Treatment with THI significantly increased both EPSCs decay time and EPSCs charge, carried by a single synaptic event in HD neurons (Fig. 2N-P). No changes were observed in EPSC frequency, amplitude and rise time (Fig. S1A-C).

THI ameliorates locomotor function and increases life span in a *Drosophila Melanogaster* HD model

HD flies (genotype: elav□Gal4/+; UAS□HttFL□Q128/+), expressing human htt cDNA encoding for full length mHtt protein (Q128HD□FL), are characterized by a progressive age-dependent motor dysfunctions and coordination difficulties (Di Cristo et al., 2020; Marsh et al., 2003).
In order to assess any potential effect of THI on both lifespan and locomotor functions, Q128HD-FL transgenic flies were fed with either 50 μM THI-supplemented AF-medium or a control diet, with the Assay fly Food (AF) medium as control.
Dietary THI significantly improved locomotor performance, as assessed by negative geotaxis assay (Fig. 3A), and significantly extended lifespan in HD flies (Fig. 3B-C).

THI treatment modulates the expression of sphingolipid metabolizing enzymes and restores normal levels of hexosylceramides in HD mice

Evidence indicates that treatment with THI may increase levels of S1P in both brain and peripheral organs (Baranowska et al., 2020; Gorshkova et al., 2013; Yu et al., 2010).
Mass spectrometry analysis has not shown changes in the levels of S1P, sphingosine (Sph) and ceramides (Cer) neither in the striatal (Fig. 4A-C) nor in the cortical (Fig. S2A-C) tissues from HD mice. Conversely, while S1P did not change, levels of both sphingosine and some ceramide species were significantly increased in brain tissues of WT controls (Fig. S2D-I).
qPCR analysis revealed that THI preserved normal expression of ceramide synthases *CerS1* and *CerS2* (Fig. 4D-E) and serine palmitoyltransferase long chain base subunit 1 *Sptlc1* (Fig. 4F), one of the enzymes involved in the *de novo* synthesis of sphingolipids, previously described reduced in the striatum of HD mice (Di Pardo et al., 2017b).
Importantly, as reported in Figure 4G, analysis of the striatum revealed that THI restored normal levels of hexosylceramides (HexCer) C18:0 and C24:1 in HD mice. Conversely, no changes were observed for HexCer C16:0 and C18:1.
Analysis of the cortex, similarly to the striatum, showed that THI restored normal levels of HexCer C18:0 (Fig. S2L). However, no effects were observed for HexCer C16:1, C18:1 and 24:1 (Fig.

S2L). WT animals did not display any variation in the striatum (Fig. S2M) nor in the cortex (Fig. S2N).

Since the mass spectrometry analysis did not clarify whether the increase in hexosylceramides was attributable to glucosylceramide (GluCer), galactosylceramide (GalCer) or both of them, we performed a semiquantitative analysis, for assessing levels of GluCer in mouse brain tissues. Immunoblotting (Slot blotting) analysis, performed by using a specific antibody against GluCer (D'Angelo et al., 2007), showed increased levels of GluCer in striatal tissues of R6/2 mice compared to WT littermates (Fig. S2O).

Finally, to establish whether GluCer accumulation was due to any change in the expression of its metabolizing enzymes, we assessed the expression of GluCer synthase (*Ugcg*) and glucocerebrosidase beta 1 and 2 enzymes (*Gba1/2*), classically involved in the GluCer degradation (Futerman and Platt, 2017).

Treatment with THI restored normal mRNA levels of *Ugcg* (Fig. 4H) and, significantly increased the expression of *Gba1* (Fig. 4I) in the striatum of HD mice compared to WT littermates. No changes in *Gba2* were observed (Fig. 4L).

Defects in HexCer metabolism are detectable early in the disease course in different HD mouse models

To possible clarify whether the accumulation of hexosylceramides might occur early in the disease, we assessed their levels in pre-manifest (4-week-old) R6/2 mice and age-matched WT littermates. As reported in Figure 5A, mass spectrometry analysis revealed that HexCer C24:1 was already increased in the striatum of 4-week-old HD mice. No difference was observed in the cortex (Fig. S3A).

Next, we assessed whether such alteration was associated with any defect in the expression of GluCer metabolizing enzymes. qPCR analysis revealed no difference in the expression profile of *Ugcg*, *Gba1* and *Gba2* (Fig. 5B-D).

Finally, in order to establish whether these defects were common to other HD mouse models, we carried out a semi-quantitative analysis of GluCer in both striatal and cortical tissues from early manifest heterozygous zQ175 (20-week-old) and transgenic YAC128 (13-week-old) HD mice. Slot blot analysis showed a significant increase in GluCer content in the cortical lysates of both HD mouse models with the respect to the WT littermates (Fig. 5E-F), whereas no changes were observed in the striatum (Fig. S3B-C).

Both deficiency of wtHtt and overexpression of mutant exon-1 fragments increase GluCer levels *in vitro*

In the attempt to clarify any potential role that Htt may have in the (dys)regulation of the GluCer metabolism, we determined GluCer content and investigated gene expression profile of metabolizing enzymes in mouse immortalized striatal-derived cell lines, expressing endogenous levels of either wt (STHdh$^{7/7}$) or mutant (STHdh$^{111/111}$) Htt.

STHdh$^{111/111}$ cells displayed increased levels of GluCer when compared to STHdh$^{7/7}$ (Figure 6A). The accumulation of GluCer was associated with reduced *Ugcg* and increased *Gba1* mRNA levels (Fig. 6B-C). No statistically significant changes were observed in *Gba2* mRNA expression (Fig. 6D).

Next, we investigated whether Htt might regulates GluCer pathways. STHdh$^{7/7}$ cells were, therefore, transiently transfected with either control or Htt siRNAs. 48 hours after transfections, the reduction of wtHtt (Fig. 6E) was associated with increased levels of GluCer (Figure 6F) without influencing on *Ugcg* or *Gba1*/*2* gene expression (Figure 6G-I).

Finally, we explored any possible effect that ectopic expression of mHtt exon-1 fragments might have in WT cells.

STHdh$^{7/7}$ were transiently transfected with the EGFP-mHtt exon-1 fragment-expressing plasmid. Similarly to what observed in the wtHtt lowering experiments, overexpression of mHtt fragments correlated with a significant increase of GluCer levels (Fig. 6L-M), suggesting that mHtt may conceivably affect the function of wt protein.

THI treatment modulates the expression of vesicle trafficking/autophagic markers and reduces Htt aggregation

In light of evidence demonstrating the ability of THI to increase the expression of the lysosomal *Gba1* enzyme (Futerman and Platt, 2017) and, considering the association between (glyco)sphingolipids and intracellular trafficking as well as endomembrane system (Futerman, 2006; Holthuis et al., 2001; Lippincott-Schwartz and Phair, 2010), the potential effect of THI on the expression of endomembrane markers in the striatum of R6/2 mice was investigated.

As reported in Figure 7A-B, THI reduced the expression of the trans GOLGI network marker, TGN38, with no effect on the cis marker GM130. Moreover, the treatment significantly increased the expression of LAMP2 (lysosome-associated membrane glycoprotein 2) (Fig. 7C), which usually maintains lysosomal stability and participates in the autophagic pathway (Morell et al., 2016; Saftig and Klumperman, 2009).

THI-mediated stimulation of the autophagic flux was confirmed by the modulation of the expression of LC3 and Beclin1 (Fig. 7D-E), two specific marker proteins of autophagy (Loeffler, 2019).

Stimulation of lysosomal/autophagic machinery has been, previously, associated with reduction of mHtt aggregation (Jarosińska and Rüdiger, 2021), classically reported as a hallmark of the disease (Reiner et al., 2011). Here therefore we explored whether THI might have any effect on protein aggregation.

Immunohistochemical (IHC) analysis revealed that treatment with THI reduced the number of mHtt EM48 positive nuclear inclusions in the striatum of R6/2 mice (Fig. 7F-G).

This result was further confirmed by immunoblotting analysis in which EM48-positive SDS-insoluble mHtt aggregates were barely detectable in HD striatal protein lysate (Fig. 7H) after treatment.

Evidence indicates that mHtt aggregates may contain also wtHtt (Cattaneo et al., 2001; Kim and Kim, 2014; Li et al., 2016; Narain et al., 1999; Nucifora et al., 2001; Riguet et al., 2021; Wheeler et al., 2000). Here, we reported the presence of nuclear inclusion of wtHtt with a distribution pattern similar to that observed for EM48-positive mHtt aggregates in the striatum of HD mice (Fig.7I). In order to better understand whether the potential coexistence of the two species of Htt might be the result of any interaction, immunoprecipitation studies were carried out.

After mHtt immunoprecipitation, by using the EM48 antibody, immunoblotting analysis with the mab2166 antibody, which recognizes a protein epitope does not present in the mutant protein (Cong et al., 2005; Fodale et al., 2020; Hensman Moss et al., 2017), highlighted the presence of wtHtt in the stacking part of the gel, where mHtt aggregates classically are trapped (Fig. 7M-N).

Administration of THI reduced mHtt aggregation and interestingly, diminished also the number of wtHtt nuclear inclusion (Fig. 7L), that contextually resulted in a detectable increased expression of soluble full-length wtHtt, (Fig.7M-N) in the striatal tissues of HD mice. This result suggested a potential augmented bioavailability of “free” wt protein after THI.

Discussion

In this study, we demonstrated that chronic infusion of THI, an inhibitor of the S1P degradative enzyme, SGPL1, resulted therapeutically effective in two experimental models of HD.

Importantly, we also reported, for the first time, that Htt protein plays a key role in the regulation of levels of some glycosphingolipid species.

The evidence of THI in evoking the activation of neuroprotective pathways and counteracting both the reduction of BDNF and the abnormal increase of mHtt aggregates, classically reported as two

hallmarks of the disease (Reiner et al., 2011), highlighted its disease-modifying properties in HD. THI administration was also associated with preservation of white matter integrity and amelioration of synaptic activity.

The beneficial effects observed in *Drosophila Melanogaster* HD model further highlighted the therapeutic potential of the compound.

Under the metabolic point of view, THI evoked a number of different events, including the modulation of (glyco)sphingolipid pathways. Mass spectrometry, however, did not reveal variation in S1P content in brain tissues. The reasons we failed to detect any increment in S1P bioavailability are not clear but may be multiple.

Evidence indicates that full body SGPL1-deficient mice show increased levels of S1P in several tissues except the brain (Billich et al., 2013) and suggests that this enzyme may not be the only key regulator of S1P levels in the brain as in other tissues (Billich et al., 2013). Given the complexity of S1P metabolism, other enzymes, such as SPHK1/2, may play a role in the brain.

On the other hand, other aspects may be considered. Recently it has been reported that i.p. injection of the 3 mg/kg THI, for one week, was able to increase levels of S1P in the brain of streptozotocin-diabetic rats (Baranowska et al., 2020). Here, we used the lowest concentration (0.1 mg/kg) of the inhibitor, reported to be safe *in-vivo* (GOBIN and PHILLIPS, 1991). Thus, we can speculate that, due to our experimental conditions (duration of treatment and concentration of the compound), any small variation of S1P, eventually induced by THI, may be not easily detectable in brain tissues.

Nevertheless, the evidence that THI normalized the expression of the enzymes involved in the synthesis of sphingolipids, including the *de novo* pathways, suggests that the compound is potentially able to modulate the metabolic routes.

Indeed, the treatment restored normal levels of some hexosylceramide species, which were found to be increased in both *in vitro* and *in vivo* experimental models.

Although, we cannot establish whether both GluCer and GalCer levels were increased in R6/2 mice, by mass spectrometry, the semiquantitative analysis, performed both *in vitro* and *in vivo*, suggested that HD models are characterized by an accumulation of GluCer, as recently reported in HD human post mortem brains (Hunter et al., 2021).

Accumulation of GluCer occurs in other neurodegenerative disorders (Bouscary et al., 2021; Indellicato and Trinchera, 2019) and it is usually attributable to either the deficient activity of lysosomal GBA1 or to the up-regulation of UGCG (Do et al., 2019; Dodge et al., 2015; Henriques et al., 2015).

In this study we did not measure any enzymatic activity, however our findings showed that accumulation of GluCer was associated with a reduced expression of *Ugcg* only in manifest R6/2 mice.

Although pre-manifest R6/2 mice, displayed accumulation of HexCer, no defective gene expression was observed early in the disease. This result suggests that the alteration, detected at symptomatic stages of the disease, may be secondary to the glycolipid accumulation. Thus, it is plausible that the accumulation of GluCer may not be a mere consequence of the progression of the neurodegenerative processes, but rather it could represent a factor contributing to the pathogenesis of HD.

Our findings suggest that wtHtt may have a critical role in the regulation of GluCer levels. This is supported by the evidence that either the over-expression of mHtt-exon1 fragments or the loss of function of wtHtt exert similar effects in increasing GluCer levels, suggesting that mutant fragments may interfere with the normal function of the wt protein, through a possible "dominant negative" action (Li et al., 2016).

A number of studies indicates that mHtt inclusions can trap normal-length polyglutamine-containing proteins, including wtHtt, and affect their functions (Cattaneo et al., 2001; Kim and Kim, 2014; Li et al., 2016; Narain et al., 1999; Nucifora et al., 2001; Riguet et al., 2021; Wheeler et al., 2000). Our findings are in line with this concept and similarly to the mutant protein, wtHtt was found accumulated in the nuclei of striatal cells in R6/2 mice.

THI, by modulating sphingolipid metabolism, stimulates autophagic and lysosomal machinery and promote the normalization of GluCer content. To this regard, in the contest of HD, the stimulation of autophagic pathways may facilitate the reduction of Htt aggregates and eventually increase levels of "free" wt protein allowing the "re-establishment" of its physiological functions, eventually contributing to the maintenance of glycosphingolipid homeostasis, through a possible positive feedback mechanism.

Evidence demonstrates that accumulation of GluCer is attributable to an abnormal endomembrane homeostasis and altered lipid recycling in different diseases (Abdul-Hammed et al., 2017; Parenti et al., 2021). We believe that such GluCer accumulation in HD, may depend on the effect that mHtt has on the regulation of endomembrane and vesicle trafficking (Caviston and Holzbaur, 2009; Wanker et al., 2019).

In conclusion, our findings further support the concept that the alteration of (glyco)sphingolipid pathways may contribute to the pathogenesis of the disease and may be eventually pharmacologically targeted. This is supported by the evidence that some drugs, including THI derivatives, whose molecular targets belong to these pathways, are already in clinical trial for

different other diseases (Canals and Clarke, 2021; Chew et al., 2016; Nabizadeh et al., 2018; O'Sullivan and Dev, 2017) and could be eventually repurposed for the treatment of HD and/or serve as a tool for the development of new ones.

Acknowledgments

We thank Enrico Amico, Susy Giova e Salvatore Castaldo for technical assistance. This study was funded by Telethon Grant GGP20101 to V.M and by EHDN Project # 903 to A.D.P. This study was supported by Fondazione Neuromed.

Author contributions

V.M. conceived the study and designed the experiments. G.P., L.C., F.M., N.R., A.S., P.L., K.M., T.F.B., T.J.B., P.S. and C.D.C. performed the experiments. A.A., A.B., F.A.D., S.F., F.F., R.P. supervised the experiments and contributed to the manuscript preparation. All authors contributed to data analysis and interpretation. V.M., A.D.P. and G.P. wrote the manuscript.

Declaration of interests

The authors declare no competing interests.

Figure legends

Figure 1. Treatment with THI mitigates motor deficit and evokes the activation of pro-survival pathways in R6/2 mice

(A-B) Limb-clasping response of vehicle- and THI-treated R6/2 mice at 11 weeks of age.

(C) Motor performance assessed by Rotarod in vehicle- and THI-treated WT and R6/2 mice. Values are represented as mean ± SD N=8 (females N=5; males N=3) for each group of mice. Two-Way ANOVA, **a**: R6/2 vehicle vs WT vehicle ****, $p < 0.0001$; R6/2 vehicle vs WT THI ****, $p < 0.0001$; R6/2 vehicle vs R6/2 THI *, $p < 0.05$; **b**: R6/2 vehicle vs WT vehicle ***, $p < 0.001$; R6/2 vehicle vs WT THI ****, $p < 0.0001$; **c**: R6/2 vehicle vs WT vehicle ****, $p < 0.0001$; R6/2 vehicle vs WT THI ****, $p < 0.0001$; R6/2 THI vs WT THI **$p < 0.01$; R6/2 vehicle vs R6/2 THI ***, $p < 0.001$; **d**: R6/2 vehicle vs WT vehicle ****, $p < 0.0001$; R6/2 vehicle vs WT THI ****, $p < 0.0001$; R6/2 THI vs WT THI *$p < 0.05$; R6/2 vehicle vs R6/2 THI ****, $p < 0.0001$; **e**: R6/2 vehicle vs WT vehicle ****, $p < 0.0001$; R6/2 vehicle vs WT THI ****, $p < 0.0001$; R6/2 vehicle vs WT THI ****, $p < 0.0001$.

(D) Motor performance assessed by Horizontal Ladder Task in vehicle- and THI-treated WT and R6/2 mice. The arrows indicate the treatment initiation. Values are represented as mean ± SD N=8

(females N=5; males N=3) for each group of mice. Two-Way ANOVA, **f**: R6/2 vehicle vs WT vehicle **p < 0.01; R6/2 THI vs WT vehicle *p < 0.05; R6/2 vehicle vs WT THI **p < 0.01; R6/2 THI vs WT THI *p < 0.05; **g**: R6/2 vehicle vs WT vehicle ****, p < 0.0001; R6/2 THI vs WT vehicle *p < 0.05; R6/2 vehicle vs WT THI ****, p < 0.0001; R6/2 vehicle vs R6/2 THI ***, p < 0.001; **h**: R6/2 vehicle vs WT vehicle ****, p < 0.0001; R6/2 THI vs WT vehicle **p < 0.01; R6/2 vehicle vs WT THI ****, p < 0.0001; R6/2 THI vs WT THI ****, p < 0.0001; R6/2 vehicle vs R6/2 THI ****, p < 0.0001; **i**: R6/2 vehicle vs WT vehicle ****, p < 0.0001; R6/2 THI vs WT vehicle ****, p < 0.0001; R6/2 vehicle vs WT THI ****, p < 0.0001; R6/2 THI vs WT THI ****, p < 0.0001; R6/2 vehicle vs R6/2 THI ****, p < 0.0001; **l**: R6/2 vehicle vs WT vehicle ****, p < 0.0001; R6/2 THI vs WT vehicle ****, p < 0.0001; R6/2 vehicle vs WT THI ****, p < 0.0001; R6/2 THI vs WT THI ****, p < 0.0001; R6/2 vehicle vs R6/2 THI ****, p < 0.0001; **m**: R6/2 vehicle vs WT vehicle ****, p < 0.0001; R6/2 THI vs WT vehicle ****, p < 0.0001; R6/2 vehicle vs WT THI ****, p < 0.0001; R6/2 THI vs WT THI ****, p < 0.0001; R6/2 vehicle vs R6/2 THI ****, p < 0.0001.

(E) Fold of change of body weight loss in vehicle- and THI-treated WT and R6/2 mice at 11 weeks of age. Values are represented as mean ± SD N=8 (females N=5; males N=3) for each group of mice. Two-Way ANOVA, *, p < 0.05; ****, p < 0.0001.

(F) Brain weight of vehicle- and THI-treated WT and R6/2 mice. Values are represented as mean ± SD N=8 (females N=5; males N=3) for each group of mice. Two-Way ANOVA, *, p < 0.05; ***, p < 0.001; ****, p < 0.0001.

(G) Representative cropped immunoblotting and densitometric of AKT kinase in striatal tissues from vehicle- and THI-treated R6/2 mice at 11 weeks of age. Values are represented as mean ± SD. N = 6 for each group of mice. Un-paired *t*-test, ***p < 0.001.

(H) Representative cropped immunoblotting and densitometric of DARPP-32 in striatal tissues from vehicle- and THI-treated R6/2 mice at 11 weeks of age. Values are represented as mean ± SD. N = 6 for each group of mice. Un-paired *t*-test, **p < 0.01.

(I) Representative cropped immunoblotting and densitometric of BDNF in striatal tissues from vehicle-treated WT and vehicle- and THI-treated R6/2 mice at 11 weeks of age. Values are represented as mean ± SD. N = 6 for each group of mice. One-Way ANOVA, *p < 0.05; **p < 0.01.

(L) Representative cropped immunoblotting and densitometric of BDNF in cortical tissues from vehicle-treated WT and vehicle- and THI-treated R6/2 mice at 11 weeks of age. In each immunoblotting, all samples were run on the same gel. Non-adjacent samples were separated by a black line. Values are represented as mean ± SD. N = 6 for each group of mice. One-Way ANOVA, ****p < 0.0001.

Figure 2. THI treatment preservers white-matter integrity and ameliorates synaptic activity in HD cortical pyramidal neurons

(A) Representative micrograph of CC thickness of Vehicle-treated WT (left), vehicle- (center) and THI-treated R6/2 (right) mice at 11 weeks of age. Scale bar: 100 μm.

(B) Semiquantitative measurement of CC thickness (μm) in correspondence of the middle line of the brain as indicated in (B). Values are represented as mean ± SD. N = 4 for each group of mice. One-Way ANOVA, ***p < 0.001; ****p < 0.0001.

(C) Representative cropped immunoblotting and densitometric of MBP in CC protein lysate from vehicle-treated WT and vehicle- and THI-treated R6/2 mice at 11 weeks of age. Values are represented as mean ± SD. N = 6 for each group of mice. One-Way ANOVA, **p < 0.01; ***p < 0.001.

(D) Representative cropped immunoblotting and densitometric of MAG in CC protein lysate from vehicle-treated WT and vehicle-and THI-treated R6/2 mice at 11 weeks of age. Values are represented as mean ± SD. N = 6 for each group of mice. One-Way ANOVA, *, p < 0.05; ***p < 0.001; ***p < 0.0001.

(E) Representative electron micrographs of axons in the CC from vehicle-treated WT and Vehicle- and THI-treated R6/2 mice at 11 weeks of age. Giant axons (left panels) are indicated by arrows. Myelin sheet abnormities (right panels) are indicated by arrowheads. Scale bar (left panels): 1 μm; Scale bar (right panels; high magnification) = 0.2 μm.

(F) Bar graphs representing the myelin thickness in the CC from vehicle-treated WT and vehicle- and THI-treated R6/2 mice at 11 weeks of age. Values are represented as mean ± SEM. N = 4 for each group of mice. Fifty axons for each experimental group. One-way ANOVA, **p<0.01; ***, p<0.001.

(G) Bar graphs representing the axon maximum diameter in the CC from vehicle-treated WT and vehicle- and THI-treated R6/2 mice at 11 weeks of age. Values are represented as mean ± SEM. N = 4 for each group of mice. Fifty axons for each experimental group. One-way ANOVA, **p < 0.01; ***, p < 0.001

(H) Bar graphs representing the axon minimum diameter in the CC from Vehicle-treated WT and vehicle- and THI-treated R6/2 mice at 11 weeks of age. Values are represented as mean ± SEM. N = 4 for each group of mice. Fifty axons for each experimental group. One-way ANOVA, **p < 0.01; ***, p < 0.001.

(I) Bear graphs representing the axon mean diameter in the CC from vehicle-treated WT and vehicle- and THI-treated R6/2 mice at 11 weeks of age. Values are represented as mean ± SEM. N

= 4 for each group of mice. Fifty axons for each experimental group. One-way ANOVA, **p < 0.01; ***, p < 0.001.

(L) Representative cropped immunoblotting and densitometric of PSD-95 in protein lysates from striatum of vehicle-treated WT and vehicle- and THI-treated R6/2 mice at 11 weeks of age. Values are represented as mean ± SD. N = 6 for each group of mice. One-Way ANOVA, *p < 0.05; **p < 0.01.

(M) Representative cropped immunoblotting and densitometric of PSD-95 in the protein lysates from cortex of vehicle-treated WT and vehicle- and THI-treated R6/2 mice at 11 weeks of age. Values are represented as mean ± SD. N = 6 for each group of mice. One-Way ANOVA, **p < 0.01; ***p < 0.005.

(N) Typical EPSC traces recorded from respectively vehicle-treated WT (black), vehicle- (light grey) and THI-Treated R6/2 mice (dark grey) at 8 weeks of age.

(O) Bar graphs representing mean of EPSC decay time$_{90\text{-}10}$ obtained from 5, 5 and 6 cells from vehicle-treated WT, vehicle- and THI-Treated R6/2 mice, respectively. One-Way ANOVA, *p < 0.05.

(P) Bar graphs representing EPSC mean of charge obtained from 5, 4 and 6 cells from WT, R6/2 untreated and R6/2 treated mice, respectively. One-Way ANOVA, *p < 0.05.

Figure 3. THI ameliorates locomotor function and increases life span in a *Drosophila Melanogaster* HD model

(A) Analysis of locomotor functions in untreated versus THI-treated HD *Drosophila Melanogaster* HD model after 12 days of treatment, as assessed by Climbing test. Values are represented as mean ± SD. Un-paired *t*-test, *p < 0.05; ***p < 0.001.

(B) Comparison of age□dependent survival curves in untreated and THI-treated HD flies. Mantel-Cox test, p < 0.0001.

(C) Percentage of medium and maximum life span change. Values are represented as mean ± SD. Un-paired *t*-test, **p < 0.01.

Figure 4. THI treatment modulates the expression of sphingolipid metabolizing enzymes and restores normal levels of hexosylceramides in HD mice

(A) Lipidomic analysis by LC-MS/MS of S1P in striatal tissues of Vehicle- and THI-treated R6/2 mice at 11 weeks of age. Values are represented as mean ± SD. N = 7 for each group of mice.

(B) Lipidomic analysis by LC-MS/MS of Sph in striatal tissues of Vehicle- and THI-treated R6/2 mice at 11 weeks of age. Values are represented as mean ± SD. N = 7 for each group of mice.

(C) Lipidomic analysis by LC-MS/MS of Cer in striatal tissues of Vehicle- and THI-treated R6/2 mice at 11 weeks of age. Values are represented as mean ± SD. N = 7 for each group of mice.
(D) qPCR analysis of *CerS1* in the striatum of vehicle-treated WT and Vehicle- and THI-treated R6/2 mice at 11 weeks of age. Values are represented as mean ± SD. N = 6 for each group of mice. One-Way ANOVA, *p < 0.05; ***, p < 0.01.
(E) qPCR analysis of *CerS2* in the striatum of vehicle-treated WT and Vehicle- and THI-treated R6/2 mice at 11 weeks of age. Values are represented as mean ± SD. N = 6 for each group of mice. One-Way ANOVA, **p < 0.01; ***, p < 0.001.
(F) qPCR analysis of *Sptlc1* in the striatum of vehicle-treated WT and Vehicle- and THI-treated R6/2 mice at 11 weeks of age. Values are represented as mean ± SD. N = 6 for each group of mice. One-Way ANOVA, *p < 0.05; **, p < 0.01.
(G) Lipidomic analysis by LC-MS/MS of HexCer 16:0, 18:0, 18:1 and 24:1 in striatal tissues of vehicle-treated WT and vehicle- and THI-treated R6/2 mice at 11weeks of age. Values are represented as mean ± SD. N = 7 for each group of mice. One-Way ANOVA, *p < 0.05; **, p < 0.01.
(H) qPCR analysis of *Ugcg* in the striatum of vehicle-treated WT and vehicle- and THI-treated R6/2 mice at 11 weeks of age. Values are represented as mean ± SD. N = 6 for each group of mice. One-Way ANOVA, **p < 0.01; ***, p < 0.01.
(I) qPCR analysis of *Gba1* in the striatum of vehicle-treated WT and vehicle- and THI-treated R6/2 mice at 11 weeks of age. Values are represented as mean ± SD. N = 6 for each group of mice. One-Way ANOVA, **p < 0.01; ***, p < 0.001.
(L) qPCR analysis of *Gba2* in the striatum of vehicle-treated WT and vehicle- and THI-treated R6/2 mice at 11 weeks of age. Values are represented as mean ± SD. N = 6 for each group of mice.

Figure 5. Defects in HexCer metabolism are detectable early in the disease course in different HD mouse models

(A) Lipidomic analysis by LC-MS/MS of HexCer 16:0, 18:0 and 24:1 in striatal tissues of pre-manifest (4-week-old) R6/2 mice and aged-matched WT littermates. Values are represented as mean ± SD. N = 4 for each group of mice. Un-paired *t*-test, *p < 0.05.
(B) qPCR analysis of *Ugcg* in striatal tissues of of pre-manifest (4-week-old) R6/2 mice and aged-matched WT littermates. Values are represented as mean ± SD. N = 6 for each group of mice.
(C) qPCR analysis of *Gba1* in in striatal tissues of pre-manifest (4-week-old) R6/2 mice and aged-matched WT littermates. Values are represented as mean ± SD. N = 6 for each group of mice.

(D) qPCR analysis of *Gba2* in striatal tissues of of pre-manifest (4-week-old) R6/2 mice and aged-matched WT littermates. Values are represented as mean ± SD. N = 6 for each group of mice.
(E) Slot-Blotting and densitometric analysis of GluCer in cortical tissues from WT and heterozygous zQ175 mice at 20 weeks of age. Values are represented as mean ± SD. N = 4 for WT mice; N = 6 for HD mice. Ponceau red was used as total protein loading control. Un-paired *t*-test, **p < 0.01.
(F) Slot-Blotting and densitometric analysis of GluCer in cortical tissues from WT and YAC128 mice at 13 weeks of age. Values are represented as mean ± SD. N = 5 for WT mice; N = 6 for HD mice. Ponceau red was used as total protein loading control. Un-paired *t*-test, **p < 0.01.

Figure 6. Both deficiency of wtHtt and overexpression of mutant exon-1 fragments increase GluCer levels *in vitro*

(A) Representative cropped Slot-Blotting and densitometric of GluCer in WT ($STHdh^{7/7}$) and HD ($STHdh^{111/111}$) total protein lysate. Values are represented as mean ± SD of four independent experiments. Ponceau red was used as total protein loading control. Un-paired *t*-test, *p < 0.05.
(B) qPCR analysis of *Ugcg* in $STHdh^{7/7}$ and $STHdh^{111/111}$ cells. Values are represented as mean ± SD of four independent experiments. Unpaired *t*-test, *p < 0.05.
(C) qPCR analysis of *Gba1* in $STHdh^{7/7}$ and $STHdh^{111/111}$ cells. Values are represented as mean ± SD of four independent experiments. Un-paired *t*-test, *p < 0.05.
(D) qPCR analysis of *Gba2* in $STHdh^{7/7}$ and $STHdh^{111/111}$ cells. Values are represented as mean ± SD of four independent experiments.
(E) Representative cropped immunoblotting and densitometric of wtHtt in $STHdh^{7/7}$ after 48 of transfection with either control (CTRL) or Htt (HTT) small interfering RNA (siRNA). Values are represented as mean ± SD of four independent experiments. Un-paired *t*-test, *p < 0.05.
(F) Representative cropped Slot-Blotting and densitometric of GluCer in $STHdh^{7/7}$ cells after 48 of transfection with either control (CTRL) or Htt (HTT) small interfering RNA (siRNA). Values are represented as mean ± SD of four independent experiments. Ponceau red was used as total protein loading control. Unpaired *t*-test, **p < 0.01.
(G) qPCR analysis of *Ugcg* in $STHdh^{7/7}$ cells after 48 of transfection with either control (CTRL) or Htt (HTT) small interfering RNA (siRNA). Values are represented as mean ± SD of four independent experiments.
(H) qPCR analysis of *Gba1* in $STHdh^{7/7}$ cells after 48 of transfection with either control (CTRL) or Htt (HTT) small interfering RNA (siRNA). Values are represented as mean ± SD of four independent experiments.

(I) qPCR analysis of *Gba2* in STHdh$^{7/7}$ cells after 48 of transfection with either control (CTRL) or Htt (HTT) small interfering RNA (siRNA). Values are represented as mean ± SD of four independent experiments.
(L) Representative cropped immunoblotting and densitometric of GluCer in STHdh$^{7/7}$ after 48 of transfection with either control (pcDNA3.1) or Htt (mHttex1) EGP-expressing construct. Values are represented as mean ± SD of four independent experiments. Ponceau red was used as total protein loading control. Un-paired *t*-test, *p < 0.05.
(M) Immunoblottings of both GFP and Actin in STHdh$^{7/7}$ cells after 48 of transfection with either control (pcDNA3.1) or Htt (mHttex1) EGP-expressing construct.

Figure 7. THI treatment modulates the expression of vesicle trafficking/autophagic markers and reduces Htt aggregation

(A) qPCR analysis of trans GOLGI marker TGN38 in striatal tissues of vehicle- and THI-treated R6/2 mice at 11 weeks of age. Values are represented as mean ± SD. N = 6 for each group of mice. Un-paired *t*-test, **p < 0.05.
(B) qPCR analysis of cis GOLGI marker GM130 in striatal tissues of vehicle- and THI-treated R6/2 mice at 11 weeks of age. Values are represented as mean ± SD. N = 6 for each group of mice.
(C) Representative cropped immunoblotting and densitometric of lysosomal marker LAMP2 in the striatum of vehicle- and THI-treated R6/2 mice at 11 weeks of age. Values are represented as mean ± SD. N = 6 for each group of mice. One-Way ANOVA, **p < 0.01.
(D) Representative cropped immunoblotting and densitometric of LC3II/LC3I in the striatum of vehicle- and THI-treated R6/2 mice at 11 weeks of age. Values are represented as mean ± SD. N = 6 for each group of mice. One-Way ANOVA, **p < 0.01
(E) Representative cropped immunoblotting and densitometric of Beclin in the striatum of vehicle- and THI-treated R6/2 mice at 11 weeks of age. Values are represented as mean ± SD. N = 6 for each group of mice. One-Way ANOVA, **p < 0.01
(F) Representative fluorescence microscopy micrograph of EM48-positive mHtt nuclear inclusions (green signal) in the striatum of vehicle- and THI-treated R6/2 mice at 11 weeks of age. Nuclei are stained with DAPI (blue signal). Scale bar: 20 μm.
(G) Semi-quantitative analysis of the number of mHtt nuclear inclusions. Data are represented as mean ± SD, N = 4 for each group of mice. Un-paired *t*-test, ****p < 0.0001.
(H) Representative cropped immunoblotting of EM48-positive mHtt aggregates in striatal lysate of vehicle- and THI-treated R6/2 mice at 11 weeks of age N = 6 for each group of mice. Values are represented as mean ± SD. Un-paired *t*-test, ***p < 0.001.

(I) Representative fluorescence microscopy micrograph of mab2166-positive wtHtt nuclear inclusions (red signal) in the striatum of vehicle- and THI-treated R6/2 mice at 11 weeks of age. Nuclei are stained with DAPI (blue signal). Scale bar: 20 μm.

(L) Semi-quantitative analysis of the number of wtHtt nuclear inclusions. Data are represented as mean ± SD, N = 4 for each group of mice. Un-paired *t*-test, ****$p < 0.0001$.

(M) Immunoblotting analysis of both SDS-insoluble and soluble wtHtt, co-immunoprecipitated with EM48 antibody, and revealed with the anti-Htt mab2166. In each immunoblotting, all samples were run on the same gel. Non-adjacent samples were separated by a black line.

(N) Immunoblotting analysis of both SDS-insoluble mHtt aggregates, co-immunoprecipitated and revealed with EM48 antibody. In each immunoblotting, all samples were run on the same gel. Non-adjacent samples were separated by a black line.

STAR Methods

REAGENT or RESOURCE	SOURCE	IDENTIFIER
Antibodies		
Rabbit polyclonal anti-DARPP-32	Cell Signaling	Cat.No. 2302
Rabbit polyclonal anti-phospho-AKT	Immunological Sciences	Cat.No. AB-10521
Rabbit monoclonal anti-AKT	Immunological Sciences	Cat.No. MAB-94320
Rabbit polyclonal anti-BDNF	Santa Cruz	Cat.No. sc-546
Mouse monoclonal anti-MBP	Cell Signaling	Cat.No. 13344
Mouse monoclonal anti-MAG	Santa Cruz	Cat.No. sc-166849
Mouse monoclonal anti-PSD-95	Millipore	Cat.No. MAB1596
Rabbit monoclonal anti-Huntingtin (D7F7)	Immunological Sciences	Cat.No. MAB-94596
Rabbit polyclonal anti-GFP	Synaptic Systems	Cat.No. 132 002
Rabbit polyclonal anti-LAMP2	Immunological Sciences	Cat.No. AB-84316
Rabbit polyclonal anti-LC3B	Sigma	Cat.No. L7543
Rabbit polyclonal anti-Beclin1	Santa Cruz	Cat.No. sc-11427
Mouse monoclonal anti-Huntingtin (EM48)	Millipore	Cat.No. MAB-5374
Mouse monoclonal anti-Huntingtin (1H-4C8)	Millipore	Cat.No. MAB2166
Rabbit anti-GluCer	Glycobiotech	Cat.No. RAS_0010
Mouse monoclonal anti-Actin	Sigma	Cat.No. A5441
Rabbit polyclonal anti-Cyclophilin	Abcam	Cat.No. ab16045
Rabbit polyclonal anti-alpha Tubulin	Abcam	Cat.No. ab4074
Goat polyclonal anti-rabbit	Millipore	Cat.No. 401315
Goat polyclonal anti-mouse	Millipore	Cat.No. 401215
Horse anti-mouse (Fluorescein)	Vector Laboratories	Cat.No. FI-2000
Donkey anti-mouse (Cy3)	Jackson Immuno Research Laboratories	Cat.No. 715-167-003
Bacterial and virus strains		
Biological samples		
Chemicals, peptides, and recombinant proteins		
THI (2-acetyl-4-(tetrahydroxybutyl)-imidazole)	Cayman	Cat:No. 13222
DMSO (Dimethyl Sulfoxide)	ChemCruz	Cat.No. sc-358801
ECL	This paper	N/A
protein G-Sepharose	Invitrogen	Cat.No. 101243
Lipofectamine LTX and Plus reagent	Invitrogen	Cat.No. 15338-100
Protease inhibitor mixture	Immunological Sciences	Cat.No. IS11041
Assay fly Food	N/A	N/A
Critical commercial assays		
Deposited data		
Experimental models: Cell lines		
Conditionally immortalized mouse striatal knock-in cells STHdh$^{7/7}$	Coriell Cell Repositories	N/A
Conditionally immortalized mouse striatal knock-in cells STHdh$^{111/111}$	Coriell Cell Repositories	N/A
Experimental models: Organisms/strains		
D. melanogaster: F1 elav-GAL4/UAS HTT128QFL (Q128HD□FL)	This paper	N/A
Mouse: R6/2: B6CBA-tgN (HDexon1) 62Gpb/1J	The Jackson Laboratory	JAX: 002810
Mouse: zQ175: B6J.129S1-*Htt*^{tm1Mfc}/190ChdiJ	The Jackson Laboratory	JAX: 027410
Mouse: YAC128: FVB-Tg(YAC128)53Hay/J mice	The Jackson Laboratory	JAX: 027432

Oligonucleotides		
Silencer™ Negative Control	Ambion	Cat.No AM4611
Silencer™ Pre-Designed siRNA (Huntingtin)	Ambion	Cat.No. AM16708
Primer: CerS1 Forward:CACACATCTTTCGGCCCCT Reverse:GCGGGTCATGGAAGAAAGGA	This paper	N/A
Primer: CerS2 Forward:GGTGGAGGTAGACCTTTTGTCA Reverse:CGGAACTTTTTGAGAAGACTGGG	This paper	N/A
Primer: Sptlc1 Forward:TACTCAGAGACCTCCAGCTG Reverse:CACCAGGGATATGCTGTCAT	This paper	N/A
Primer: Ugcg Forward:TTGTTCGGCTTGTGCTCTT Reverse: GAGACACCAGGGAGCTTGCT	This paper	N/A
Primer: Gba1 Forward: CTTCCTATTTCAGGCGGTATCTT Reverse: AGAGTCACAGTACGATGCATTA	This paper	N/A
Primer: Gba2 Forward: CACCTATCTTGCCTCATGACTAC Reverse: GAAACGTCCAGAGTCTCATCTC	This paper	N/A
Primer: TGN38 Forward: GCAGCCACTTCTTTGCATATCTAG Reverse: AGTGACTTTGGATCTTTTCCCTTC	This paper	N/A
Primer: GM130 Forward: CAGGCAGACAGGTATAACAAG Reverse: CGGAGTTTCTCTTCCAGTTC	This paper	N/A
Primer: Cyc Forward: TCCAAAGACAGCAGAAAACTTTCG Reverse: TCTTCTTGCTGGTCTTGCCATTCC	This paper	N/A
Recombinant DNA		
Plasmid: EGFP-pcDNA3.1	This paper	N/A
Plasmid: EGFP-mHttex1	This paper	N/A
Software and algorithms		
ImageJ	NIH	https://imagej.nih.gov/ij
Prism	GraphPad Software	Version 8
Other		

Animal models. All experimental procedures were approved by the IRCCS Neuromed Animal Care Review Board and by "Istituto Superiore di Sanità" (ISS permit numbers: 760/2020-PR and 433/2021-PR) and were conducted according to 2010/63/EU Directive for animal experiments. Breeding pairs of the R6/2 line of transgenic mice [strain name: B6CBA-tgN (HDexon1) 62Gpb/1J] with ~160 ± 10 (CAG) repeat expansions (Mangiarini et al., 1996) were purchased from the Jackson Laboratories (Bar Harbor, ME, USA). Htt^{tm1Mfc}/190tChdi (zQ175 knock-in) mice (CAG198) were received from the CHDI Foundation by the Jackson Laboratories. Heterozygous zQ175 knock-in mice with ~ 190 CAG repeats in a chimeric human/mouse exon 1 of the murine Htt gene (Menalled et al., 2012) and age-matched WT littermates were used. YAC128 expressing the entire human HD gene (including promoter region) with 128 CAG repeats. YAC128 mice and age-matched WT littermates were used.

Animal treatment. Analyses were carried out in both R6/2 mice and WT littermates starting from 5 weeks of age. To ensure homogeneity of experimental cohorts, mice from the same F generation were assigned to experimental groups, such that age and weight were matched.

***In-vivo* drug administration**. 2-acetyl-4-(tetrahydroxybutyl)-imidazole (THI**)** (Cayman, Cat. N. 13222) was dissolved in DMSO, further diluted in saline (vehicle) and daily administered by intraperitoneal (i.p.) injection at dose of 0.1 mg/kg (GOBIN and PHILLIPS, 1991). Control mice (WT and R6/2) were daily injected with the same volume of vehicle containing DMSO.

Clasping analysis. Clasping score was determined over 30 seconds. Mice were suspended by their tails from a height of 50 cm and a limb-clasping response was defined as the withdrawal of any limb to the torso for more than 2 seconds. The following scores were used: 0, absence of clasping; 0.5, withdrawal of any single limb; 1, withdrawal of any two limbs; 1.5, withdrawal of any three limbs; 2, withdrawal of all four limbs.

Motor behavior tests. Motor performance was assessed by Horizontal Ladder Task and Rotarod tests as previously described (Di Pardo et al., 2018).

Brain lysate preparation. Mice were sacrificed within 1 h from the last treatment by cervical dislocation and brains were removed from the skull, weighed and bisected. Brains were immediately snap-frozen in liquid N2 and pulverized in a mortar with a pestle as previously described (Di Pardo et al., 2018).

Immunoblottings. Proteins (20 μg) were resolved on 10% SDS-PAGE and immunoblotted with the following antibodies: anti-DARPP-32 (1:1000) (Cell Signaling, Cat. N. #2302), anti-phospho-AKT (1:1000) (Immunological Sciences, Cat. N. AB-10521), anti-AKT (1:1000) (Immunological Sciences, Cat. N. MAB-94320), anti-BDNF (1: 1000) (Santa Cruz, Cat. N. sc-546), anti-MBP (1:1000) (Cell Signaling, Cat. N. #13344), anti-MAG (1:1000) (Santa Cruz, Cat. N. sc-166849), anti-PSD-95 (1:1000) (Millipore, Cat. N. #MAB1596), anti-Htt (clone D7F7) (1:1000) (Immunological Sciences, Cat. N. MAB-94596), anti-GFP (1:2000) (Synaptic System, Cat. N. 132 002), anti-LAMP2 (1:1000) (Immunological Sciences, Cat. N. AB-84316), anti-LC3B (1:1000) (Sigma, Cat. N. L7543) and anti-Beclin1 (1:1000) (Santa Cruz, Cat. N. sc-11427).

For protein normalization, anti-Actin (1: 5000) (Sigma Aldrich, Cat. N. A5441), anti-Cyclophilin (1:2000) (Abcam, Cat. N. ab16045) and/or anti-alpha Tubulin (1:2000) (Abcam, Cat. N. ab4074) were used. Immunoblots were then exposed to specific HRP-conjugated secondary antibodies (Millipore, Cat. N. 401315 and 401215). Protein bands were visualized by ECL and quantified by Image Lab Software (Bio-Rad Laboratories).

For the analysis of mHtt aggregates, protein lysates (30 μg) were resolved on 8% SDS-PAGE, the entire gel, including the stacking portion, was trans-blotted over-night a 250 mV in 0.05% SDS and

16% methanol-containing transfer buffer. Membrane was immunoblotted with anti-Htt (clone EM48) antibody (1:1000) (Millipore, Cat. N. MAB5374). A monoclonal anti-mouse HRP-conjugated antibody (Millipore, Cat. N. 401215) was used as secondary antibody. Protein bands were visualized by ECL and quantified as described above.

Co-Immunoprecipitations. Immunoprecipitation (1 mg total lysate) was performed using the anti-mHtt antibodies (clone EM48) complexed to protein G-Sepharose (Invitrogen, Cat. N. 101243). The immunoprecipitated proteins were resolved on 7% SDS–PAGE, transferred overnight on PVDF membrane and detected by immunoblotting with mab2166 (1:1000) (Millipore, Cat. N. MAB2166) and EM48 (1:1000). HRP-conjugated secondary antibodies (Millipore, Cat. N. 401215) were used at 1:5000 dilution. Protein bands were detected by ECL and visualized by Quantity One software (Bio-Rad Laboratories).

Histochemical analyses. Brains were processed, embedded in paraffin wax and 10 μm coronal sections were cut. Four mice/group were used and immunostaining for mHtt and wtHtt aggregates was carried out by using a mouse anti-mHtt antibody (clone EM48) (1:150) and a mouse anti-wtHtt antibody (mab2166) (1:150) as recently described (Di Pardo et al., 2018).

For the analysis of CC, four mice/group were analyzed. The thickness of CC was measured in correspondence of the middle line of the brain as previously described (Di Pardo et al., 2014).

Transmission Electron Microscopy (TEM). Mouse brains were immersed in the fixing solution (paraformaldehyde 2.0% and glutaraldehyde 1% in 0.1 M phosphate buffer pH 7.4) overnight at 4°C. After washing in PBS (0.1 M), small blocks from corpus callosum were dissected out and post-fixed in 1% osmium tetroxide (OsO4) for 1h at 4°C. After washing in PBS samples were dehydrated in a gradient of ethanol solutions and finally embedded in epon-araldite resin. Ultrathin sections (90 nm) were cut at ultra-microtome (Leica Microsystems) to be collected on cupper grids and stained with uranyl acetate and lead citrate. Ultrathin sections were observed at electron-microscopy (Jeol JEM SX100, Jeol, Tokyo, Japan) at an acceleration voltage of 80 kV. For ultrastructural morphometry, grids containing non-serial ultra-thin sections (90 nm thick) were examined at a magnification of 6,000x. Several grids were analyzed in order to count a total of 50 axons from the corpus callosum from each experimental group. For the Ultra-structural analysis of axons, grids containing non-serial ultra-thin sections (90 nm thick) were examined at a magnification of 6,000x. Axon minimum and maximum diameter; axon mean diameter and myelin thickness were assessed.

Whole-cell recordings from L5 pyramidal neurons. Mice were anesthetized and quickly decapitated, and the brain rapidly removed to ice-cold glycerol-based artificial cerebrospinal fluid (ACSF) containing the following (in mM): glycerol 250, KCl 2.5, CaCl2 2.4, MgCl2 1.2, NaH2PO4

1.2, NaHCO3 26, glucose 11 and Na-pyruvate 0.1 (pH 7.35, aerated with 95% O2/5% CO2, 290–300 mOsm/l). Transversal slices, 350 μm in thickness, were cut with a vibratome (Leica VT 1000S) and placed in a slice incubation chamber at room temperature with oxygenated ACSF and transferred to a recording chamber within 1-6 h after slice preparation. Spontaneous postsynaptic excitatory currents (EPSCs) were recorded from L5 pyramidal neurons in temporal cortex from 8-week-old mice. Recordings were performed at 22-25°C, using Multiclamp 700A amplifier (Axon Instruments, Foster City, CA, USA), -70 mV holding potential, in the presence of bicuculline 20 μM to block $GABA_A$ receptors.

The patch pipette (3–4 MΩ) was filled with the following solution (in mM): KCl 140, HEPES 10, 1,2-bis(2-aminophenoxy)ethane-N,N,N,N-tetra-acetic acid 5, MgCl2 2, MgATP 2 (pH 7.35, with KOH)**.** ACSF had the following composition: 125 mM NaCl, 2.5 mM KCl, 2 mM $CaCl_2$, 1.25 mM NaH_2PO_4, 1 mM $MgCl_2$, 26 mM $NaHCO_3$, 10 mM glucose (pH 7.35). All drugs were purchased from Sigma.

Fly stocks. The fly strains used in this study were obtained from the Bloomington Stock Center: w*; P{UAS-HTT.128Q.FL}f27b and w*; P{w[+mW.hs]=GawB}elav[C155]. Flies were reared on standard cornmeal□agar with a 12□hr on–off light cycle at 22°C.

THI treatment and fly crosses. During the assays, flies were reared in tubes containing 2 mL of "Assay fly Food" (AF) (2% Agar, 10% Powdered yeast, 10% Sucrose, 0.1% Nipagin) or on the same AF supplemented with THI.

THI was added into the surface of AF at the final concentration of 50μM, and left under gentle agitation for 3 hours until dried. Controls were reared in AF supplemented with equal quantity of PBS, devoid of THI. Expression of polyglutamine□containing human HTT was obtained through the bipartite expression system (UAS)□GAL4 in trans-heterozygous F1 progeny generated by crossing females carrying the pan□neural driver elav□Gal4 to males carrying the UAS HTT128QFL construct at 27.5°C (Di Cristo et al., 2020). Only F1 adult females elav-GAL4/UAS HTT128QFL were used in this study.

Negative geotaxis assay. Negative geotaxis assay was carried out on F1 (Q128HD□FL) female flies on different days post eclosion, as previously described (Di Cristo et al., 2020). Briefly, groups of 20 female flies were placed in a graduated empty plastic vial (18 x 2.5 cm) and allowed to recover 30 min. Negative geotaxis was measured by recording the number of flies that climbed above the 10 cm mark within 20 s after a tap down of the flies to the bottom of the vial. This assay was repeated for the same group two times, allowing for a 4 min rest period between each trial. The number of flies per group that passed the 10 cm mark was recorded as a percentage of total flies. For each condition, three groups of 20 flies each were tested in the marked tube in three

independent experiments, and the data were expressed as an average of the replicates +/- SD (n = 180).

Life span analysis. Newly hatched F1 elav-GAL4/UAS HTT128QFL (Q128HD□FL) adult flies were collected, briefly anesthetized with CO_2, and sorted by sex. Five cohorts of 20 females were placed in vials containing AF, supplemented with or without THI, and reared at 27.5°C. They were transferred to new vials with fresh food every 2/3 days, and deaths were recorded at each transfer. The experiment ended when there were no more live flies in the vials. Lifespan was measured in two independent experiments (total n = 200) per treatment. Obtained values were used to calculate mean lifespan (mean survival days of all flies for each group), and maximum lifespan (maximum amount of days needed to reach 90% mortality) (Bovier et al., 2018, 2019).

Mass Spectrometry. Snap frozen brain tissues were transferred into glass tubes and stored at −80 °C until lipid extraction. Lipids were extracted using a modified Bligh and Dyer method as previously described (Di Pardo et al., 2017a). LC-MS/MS analyses of the samples were carried out on the Acquity UPLC system coupled with a Xevo TQ-MS triple-quadrupole mass spectrometer as previously described (Basit et al., 2015).

Cell models. Conditionally immortalized mouse striatal knock-in cells expressing endogenous levels of wild-type ($STHdh^{7/7}$) or mutant ($STHdh^{111/111}$) Htt were purchased from the Coriell Cell Repositories (Coriell Institute for Medical Research, Camden, NJ, USA) and were maintained as previously described (Di Pardo et al., 2014).

Cell transfection. In both Htt siRNA and ectopic expression of EGFP-mHtt-exon1 experiments, STHdh cell lines were transiently transfected using Lipofectamine LTX and Plus reagent (Invitrogen, Cat. N. 15338-100) and analysed 48 hours after transfection.

Cell lysates preparation. Cells were lysate in lysis buffer containing 20 mM Tris, pH 7.4, 1% Nonidet P-40, 1 mM EDTA, 20 mM NaF, 2 mM Na_3VO_4 and 1:1000 protease inhibitor mixture (Immunological Sciences, Cat. N. IS11041), sonicated with 2 x10 seconds pulses and then centrifuged for 10 min at 10 000*g*.

Semi-quantitative analysis of glucosylceramide. 5 μg of total protein lysate was spotted on nitrocellulose membrane by using a slot-blotting apparatus (Hoefer™ PR 648 Slot Blot Blotting Manifold). Membranes were then blocked in 5% milk in TBS-T and incubated with anti-GluCer antibody (D'Angelo et al., 2007) (1:1000) (Glycobiotech, Cat. N. RAS_0010). A polyclonal anti-rabbit HRP-conjugated antibody (Millipore, Cat. N. 401315) was used as secondary antibody. Protein bands were visualized by ECL and quantified as reported above. Ponceau Red staining served as a total protein loading control (Di Pardo et al., 2013).

Quantitative real time PCR (qPCR). Total RNA was extracted as previously described (Di Pardo et al., 2019) and qPCR analysis was performed on a CFX Connect Real-Time System instrument (Bio-Rad Laboratories). The following primers were used (5′–>3′): CerS1-Fw: CACACATCTTTCGGCCCCT; CerS1-Rv: GCGGGTCATGGAAGAAAGGA, CerS2-Fw: GGTGGAGGTAGACCTTTTGTCA; CerS2-Rv: CGGAACTTTTTGAGAAGACTGGG; Sptlc1-FW: TACTCAGAGACCTCCAGCTG; Sptlc1-RV: CACCAGGGATATGCTGTCAT; Ugcg-FW: TTGTTCGGCTTGTGCTCTT; Ugcg-Rv: GAGACACCAGGGAGCTTGCT; Gba1-FW: CTTCCTATTTCAGGCGGTATCTT; Gba1-RV: AGAGTCACAGTACGATGCATTA; Gba2-FW: CACCTATCTTGCCTCATGACTAC; Gba2-RV: GAAACGTCCAGAGTCTCATCTC; TGN38-FW: GCAGCCACTTCTTTGCATATCTAG; TGN38-RV: AGTGACTTTGGATCTTTTCCCTTC; GM-130 FW: CAGGCAGACAGGTATAACAAG; GM130-RV: CGGAGTTTCTCTTCCAGTTC; Cyc-Fw: TCCAAAGACAGCAGAAAACTTTCG; Cyc-Rv: TCTTCTTGCTGGTCTTGCCATTCC.

Statistics. Two-way ANOVA followed by Bonferroni post-test was used to compare treatment groups with the Horizontal Ladder Task and Rotarod tests as well as for the analysis of body weight gain. Mantel-Cox test was used for the fly lifespan. One-way ANOVA and Two-tailed Un-paired *t*-test were used in all other experiments, as indicated.

All data were expressed as mean ± SD except in the electrophysiological studies and TEM analyses in which data were expressed as mean ± SEM.

References

Abdul-Hammed, M., Breiden, B., Schwarzmann, G., and Sandhoff, K. (2017). Lipids regulate the hydrolysis of membrane bound glucosylceramide by lysosomal β-glucocerebrosidase. J. Lipid Res. *58*, 563–577.

Alam, S., Piazzesi, A., Abd El Fatah, M., Raucamp, M., and van Echten-Deckert, G. (2020). Neurodegeneration Caused by S1P-Lyase Deficiency Involves Calcium-Dependent Tau Pathology and Abnormal Histone Acetylation. Cells *9*.

Ayub, M., Jin, H.K., and Bae, J.S. (2021). Novelty of sphingolipids in the central nervous system physiology and disease: Focusing on the sphingolipid hypothesis of neuroinflammation and neurodegeneration. Int. J. Mol. Sci. *22*.

Baranowska, U., Holownia, A., Chabowski, A., and Baranowski, M. (2020). Pharmacological inhibition of sphingosine-1-phosphate lyase partially reverses spatial memory impairment in streptozotocin-diabetic rats. Mol. Cell. Neurosci. *107*.

Basit, A., Piomelli, D., and Armirotti, A. (2015). Rapid evaluation of 25 key sphingolipids and phosphosphingolipids in human plasma by LC-MS/MS. Anal. Bioanal. Chem. *407*, 5189–5198.

Bichell, T.J.V., Wegrzynowicz, M., Tipps, K.G., Bradley, E.M., Uhouse, M.A., Bryan, M., Horning, K., Fisher, N., Dudek, K., Halbesma, T., et al. (2017). Reduced bioavailable manganese causes striatal urea cycle pathology in Huntington's disease mouse model. Biochim. Biophys. Acta - Mol. Basis Dis. *1863*.

Billich, A., Baumruker, T., Beerli, C., Bigaud, M., Bruns, C., Calzascia, T., Isken, A., Kinzel, B., Loetscher, E., Metzler, B., et al. (2013). Partial deficiency of sphingosine-1-phosphate lyase confers protection in experimental autoimmune encephalomyelitis. PLoS One *8*.

Blaho, V.A. (2020). Druggable Sphingolipid Pathways: Experimental Models and Clinical Opportunities. Adv. Exp. Med. Biol. *1274*, 101–135.

Bouscary, A., Quessada, C., René, F., Spedding, M., Turner, B.J., Henriques, A., Ngo, S.T., and Loeffler, J.P. (2021). Sphingolipids metabolism alteration in the central nervous system: Amyotrophic lateral sclerosis (ALS) and other neurodegenerative diseases. Semin. Cell Dev. Biol. *112*, 82–91.

Bovier, T.F., Rossi, S., Mita, D.G., and Digilio, F.A. (2018). Effects of the synthetic estrogen 17-α-ethinylestradiol on Drosophila melanogaster: Dose and gender dependence. Ecotoxicol. Environ. Saf. *162*, 625–632.

Bovier, T.F., Cavaliere, D., Colombo, M., Peluso, G., Giordano, E., and Digilio, F.A. (2019). Methods to Test Endocrine Disruption in Drosophila melanogaster. J. Vis. Exp. *2019*.

Canals, D., and Clarke, C.J. (2021). Compartmentalization of Sphingolipid metabolism:

Implications for signaling and therapy. Pharmacol. Ther. 108005.
Cattaneo, E., Rigamonti, D., Goffredo, D., Zuccato, C., Squitieri, F., and Sipione, S. (2001). Loss of normal huntingtin function: new developments in Huntington's disease research. Trends Neurosci. *24*, 182–188.
Caviston, J.P., and Holzbaur, E.L.F. (2009). Huntingtin as an essential integrator of intracellular vesicular trafficking. Trends Cell Biol. *19*, 147–155.
Chew, W.S., Wang, W., and Herr, D.R. (2016). To fingolimod and beyond: The rich pipeline of drug candidates that target S1P signaling. Pharmacol. Res. *113*, 521–532.
Chuang, C.L., and Demontis, F. (2021). Systemic manifestation and contribution of peripheral tissues to Huntington's disease pathogenesis. Ageing Res. Rev. *69*.
Cong, S.Y., Pepers, B.A., Roos, R.A.C., Van Ommen, G.J.B., and Dorsman, J.C. (2005). Epitope mapping of monoclonal antibody 4C8 recognizing the protein huntingtin. Hybridoma (Larchmt). *24*, 231–235.
D'Angelo, G., Polishchuk, E., Tullio, G. Di, Santoro, M., Campli, A. Di, Godi, A., West, G., Bielawski, J., Chuang, C.C., Van Der Spoel, A.C., et al. (2007). Glycosphingolipid synthesis requires FAPP2 transfer of glucosylceramide. Nature *449*, 62–67.
Denny, C.A., Desplats, P.A., Thomas, E.A., and Seyfried, T.N. (2010). Cerebellar lipid differences between R6/1 transgenic mice and humans with Huntington's disease. J. Neurochem. *115*, 748–758.
Desplats, P.A., Denny, C.A., Kass, K.E., Gilmartin, T., Head, S.R., Sutcliffe, J.G., Seyfried, T.N., and Thomas, E.A. (2007). Glycolipid and ganglioside metabolism imbalances in Huntington's disease. Neurobiol. Dis. *27*, 265–277.
Di Cristo, F., Calarco, A., Digilio, F.A., Sinicropi, M.S., Rosano, C., Galderisi, U., Melone, M.A.B., Saturnino, C., and Peluso, G. (2020). The Discovery of Highly Potent THP Derivatives as OCTN2 Inhibitors: From Structure-Based Virtual Screening to In Vivo Biological Activity. Int. J. Mol. Sci. *21*, 1–19.
Di Paola, M., Phillips, O.R., Sanchez-Castaneda, C., Di Pardo, A., Maglione, V., Caltagirone, C., Sabatini, U., and Squitieri, F. (2014). MRI measures of corpus callosum iron and myelin in early Huntington's disease. Hum. Brain Mapp. 35.
Di Pardo, A., Alberti, S., Maglione, V., Amico, E., Cortes, E.P., Elifani, F., Battaglia, G., Busceti, C.L., Nicoletti, F., Vonsattel, J.P.G., et al. (2013). Changes of peripheral TGF-β1 depend on monocytes-derived macrophages in Huntington disease. Mol. Brain 6.
Di Pardo, A., Amico, E., Favellato, M., Castrataro, R., Fucile, S., Squitieri, F., and Maglione, V. (2014). FTY720 (fingolimod) is a neuroprotective and disease-modifying agent in cellular and mouse models of huntington disease. Hum. Mol. Genet. 23.

Di Pardo, A., Amico, E., and Maglione, V. (2016). Impaired levels of gangliosides in the corpus callosum of Huntington disease animal models. Front. Neurosci. 10.
Di Pardo, A., Amico, E., Basit, A., Armirotti, A., Joshi, P., Neely, D.M., Vuono, R., Castaldo, S., Digilio, A.F., Scalabrì, F., et al. (2017a). Defective Sphingosine-1-phosphate metabolism is a druggable target in Huntington's disease. Sci. Rep. 7.
Di Pardo, A., Basit, A., Armirotti, A., Amico, E., Castaldo, S., Pepe, G., Marracino, F., Buttari, F., Digilio, A.F., and Maglione, V. (2017b). De novo Synthesis of Sphingolipids Is Defective in Experimental Models of Huntington's Disease. Front. Neurosci. 11.
Di Pardo, A., and Maglione, V. (2018). The S1P Axis: New Exciting Route for Treating Huntington's Disease. Trends Pharmacol. Sci. *39*.
Di Pardo, A., Castaldo, S., Amico, E., Pepe, G., Marracino, F., Capocci, L., Giovannelli, A., Madonna, M., van Bergeijk, J., Buttari, F., et al. (2018b). Stimulation of S1PR <inf>5</inf> with A-971432, a selective agonist, preserves blood-brain barrier integrity and exerts therapeutic effect in an animal model of Huntington's disease. Hum. Mol. Genet. 27.
Di Pardo, A., Pepe, G., Castaldo, S., Marracino, F., Capocci, L., Amico, E., Madonna, M., Giova, S., Jeong, S.K., Park, B.M., et al. (2019). Stimulation of Sphingosine Kinase 1 (SPHK1) Is Beneficial in a Huntington's Disease Pre-clinical Model. Front. Mol. Neurosci. 12.
Do, J., McKinney, C., Sharma, P., and Sidransky, E. (2019). Glucocerebrosidase and its relevance to Parkinson disease. Mol. Neurodegener. *14*.
Dodge, J.C., Treleaven, C.M., Pacheco, J., Cooper, S., Bao, C., Abraham, M., Cromwell, M., Sardi, S.P., Chuang, W.L., Sidman, R.L., et al. (2015). Glycosphingolipids are modulators of disease pathogenesis in amyotrophic lateral sclerosis. Proc. Natl. Acad. Sci. U. S. A. *112*, 8100–8105.
Dumas, E.M., Van Den Bogaard, S.J.A., Ruber, M.E., Reilman, R.R., Stout, J.C., Craufurd, D., Hicks, S.L., Kennard, C., Tabrizi, S.J., Van Buchem, M.A., et al. (2012). Early changes in white matter pathways of the sensorimotor cortex in premanifest Huntington's disease. Hum. Brain Mapp. *33*, 203–212.
Van Echten-Deckert, G., Hagen-Euteneuer, N., Karaca, I., and Walter, J. (2014). Sphingosine-1-phosphate: Boon and bane for the brain. Cell. Physiol. Biochem. *34*, 148–157.
Ehrlich, M.E. (2012). Huntington's disease and the striatal medium spiny neuron: cell-autonomous and non-cell-autonomous mechanisms of disease. Neurotherapeutics *9*, 270–284.
Estevez-Fraga, C., Scahill, R., Rees, G., Tabrizi, S.J., and Gregory, S. (2020). Diffusion imaging in Huntington's disease: comprehensive review. J. Neurol. Neurosurg. Psychiatry *92*, 62–69.
Fodale, V., Pintauro, R., Daldin, M., Altobelli, R., Spiezia, M.C., Bisbocci, M., Macdonald, D., and Bresciani, A. (2020). Analysis of mutant and total huntingtin expression in Huntington's disease

murine models. Sci. Rep. *10*.
Futerman, A.H. (2006). Intracellular trafficking of sphingolipids: Relationship to biosynthesis. Biochim. Biophys. Acta - Biomembr. *1758*, 1885–1892.
Futerman, A.H., and Platt, F.M. (2017). The metabolism of glucocerebrosides - From 1965 to the present. Mol. Genet. Metab. *120*, 22–26.
Gatto, R.G., Weissmann, C., Amin, M., Angeles-López, Q.D., García-Lara, L., Castellanos, L.C.S., Deyoung, D., Segovia, J., Mareci, T.H., Uchitel, O.D., et al. (2021). Evaluation of early microstructural changes in the R6/1 mouse model of Huntington's disease by ultra-high field diffusion MR imaging. Neurobiol. Aging *102*, 32–49.
GOBIN, S.J.P., and PHILLIPS, J.A. (1991). Immunosuppressive effects of 2-acetyl-4-tetrahydroxybutyl imidazole (THI) in the rat. Clin. Exp. Immunol. *85*, 335–340.
Gorshkova, I.A., Wang, H., Orbelyan, G.A., Goya, J., Natarajan, V., Beiser, D.G., Vanden Hoek, T.L., and Berdyshev, E. V. (2013). Inhibition of sphingosine-1-phosphate lyase rescues sphingosine kinase-1-knockout phenotype following murine cardiac arrest. Life Sci. *93*, 359–366.
Grassi, S., Mauri, L., Prioni, S., Cabitta, L., Sonnino, S., Prinetti, A., and Giussani, P. (2019). Sphingosine 1-Phosphate Receptors and Metabolic Enzymes as Druggable Targets for Brain Diseases. Front. Pharmacol. *10*.
Hagen, N., Van Veldhoven, P.P., Proia, R.L., Park, H., Merrill, A.H., and Van Echten-Deckert, G. (2009). Subcellular origin of sphingosine 1-phosphate is essential for its toxic effect in lyase-deficient neurons. J. Biol. Chem. *284*, 11346–11353.
Hagen, N., Hans, M., Hartmann, D., Swandulla, D., and Van Echten-Deckert, G. (2011). Sphingosine-1-phosphate links glycosphingolipid metabolism to neurodegeneration via a calpain-mediated mechanism. Cell Death Differ. *18*, 1356–1365.
Henriques, A., Croixmarie, V., Priestman, D.A., Rosenbohm, A., Dirrig-Grosch, S., D'Ambra, E., Huebecker, M., Hussain, G., Boursier-Neyret, C., Echaniz-Laguna, A., et al. (2015). Amyotrophic lateral sclerosis and denervation alter sphingolipids and up-regulate glucosylceramide synthase. Hum. Mol. Genet. *24*, 7390–7405.
Hensman Moss, D.J., Robertson, N., Farmer, R., Scahill, R.I., Haider, S., Tessari, M.A., Flynn, G., Fischer, D.F., Wild, E.J., Macdonald, D., et al. (2017). Quantification of huntingtin protein species in Huntington's disease patient leukocytes using optimised electrochemiluminescence immunoassays. PLoS One *12*.
Holthuis, J.C.M., Pomorski, T., Raggers, R.J., Sprong, H., and Van Meer, G. (2001). The organizing potential of sphingolipids in intracellular membrane transport. Physiol. Rev. *81*, 1689–1723.

Hunter, M., Demarais, N.J., Faull, R.L.M., Grey, A.C., and Curtis, M.A. (2021). An imaging mass spectrometry atlas of lipids in the human neurologically normal and Huntington's disease caudate nucleus. J. Neurochem. *157*, 2158–2172.

Indellicato, R., and Trinchera, M. (2019). The Link between Gaucher Disease and Parkinson's Disease Sheds Light on Old and Novel Disorders of Sphingolipid Metabolism. Int. J. Mol. Sci. *20*.

Jarosińska, O.D., and Rüdiger, S.G.D. (2021). Molecular Strategies to Target Protein Aggregation in Huntington's Disease. Front. Mol. Biosci. *8*.

Kim, E., and Sheng, M. (2004). PDZ domain proteins of synapses. Nat. Rev. Neurosci. *5*, 771–781.

Kim, S., and Kim, K.-T. (2014). Therapeutic Approaches for Inhibition of Protein Aggregation in Huntington's Disease. Exp. Neurobiol. *23*, 36–44.

Li, L., Liu, H., Dong, P., Li, D., Legant, W.R., Grimm, J.B., Lavis, L.D., Betzig, E., Tjian, R., and Liu, Z. (2016). Real-time imaging of Huntingtin aggregates diverting target search and gene transcription. Elife *5*.

Lippincott-Schwartz, J., and Phair, R.D. (2010). Lipids and Cholesterol as Regulators of Traffic in the Endomembrane System. Annu. Rev. Biophys. *39*, 559.

Loeffler, D.A. (2019). Influence of Normal Aging on Brain Autophagy: A Complex Scenario. Front. Aging Neurosci. *11*.

Maceyka, M., Harikumar, K.B., Milstien, S., and Spiegel, S. (2012). Sphingosine-1-phosphate signaling and its role in disease. Trends Cell Biol. *22*, 50–60.

Maglione, V., Marchi, P., Di Pardo, A., Lingrell, S., Horkey, M., Tidmarsh, E., and Sipione, S. (2010). Impaired ganglioside metabolism in Huntington's disease and neuroprotective role of GM1. J. Neurosci. *30*.

Mangiarini, L., Sathasivam, K., Seller, M., Cozens, B., Harper, A., Hetherington, C., Lawton, M., Trottier, Y., Lehrach, H., Davies, S.W., et al. (1996). Exon 1 of the HD gene with an expanded CAG repeat is sufficient to cause a progressive neurological phenotype in transgenic mice. Cell *87*, 493–506.

Marsh, J.L., Pallos, J., and Thompson, L.M. (2003). Fly models of Huntington's disease. Hum. Mol. Genet. *12 Spec No 2*.

Matamales, M., Bertran-Gonzalez, J., Salomon, L., Degos, B., Deniau, J.M., Valjent, E., Hervé, D., and Girault, J.A. (2009). Striatal medium-sized spiny neurons: identification by nuclear staining and study of neuronal subpopulations in BAC transgenic mice. PLoS One *4*.

Menalled, L.B., Kudwa, A.E., Miller, S., Fitzpatrick, J., Watson-Johnson, J., Keating, N., Ruiz, M., Mushlin, R., Alosio, W., McConnell, K., et al. (2012). Comprehensive behavioral and molecular characterization of a new knock-in mouse model of Huntington's disease: zQ175. PLoS One *7*.

Mitroi, D.N., Deutschmann, A.U., Raucamp, M., Karunakaran, I., Glebov, K., Hans, M., Walter, J., Saba, J., Gräler, M., Ehninger, D., et al. (2016). Sphingosine 1-phosphate lyase ablation disrupts presynaptic architecture and function via an ubiquitin- proteasome mediated mechanism. Sci. Rep. *6*.

Mitroi, D.N., Karunakaran, I., Gräler, M., Saba, J.D., Ehninger, D., Ledesma, M.D., and van Echten-Deckert, G. (2017). SGPL1 (sphingosine phosphate lyase 1) modulates neuronal autophagy via phosphatidylethanolamine production. Autophagy *13*, 885–899.

Morell, C., Bort, A., Vara-Ciruelos, D., Ramos-Torres, Á., Altamirano-Dimas, M., Díaz-Laviada, I., and Rodríguez-Henche, N. (2016). Up-Regulated Expression of LAMP2 and Autophagy Activity during Neuroendocrine Differentiation of Prostate Cancer LNCaP Cells. PLoS One *11*.

Moruno-Manchon, J.F., Uzor, N.E., Blasco-Conesa, M.P., Mannuru, S., Putluri, N., Furr-Stimming, E.E., and Tsvetkov, A.S. (2017). Inhibiting sphingosine kinase 2 mitigates mutant Huntingtin-induced neurodegeneration in neuron models of Huntington disease. Hum. Mol. Genet. *26*, 1305–1317.

Moruno Manchon, J.F., Uzor, N.E., Dabaghian, Y., Furr-Stimming, E.E., Finkbeiner, S., and Tsvetkov, A.S. (2015). Cytoplasmic sphingosine-1-phosphate pathway modulates neuronal autophagy. Sci. Rep. *5*.

Nabizadeh, A., Amani, B., Kadivar, M., Toroski, M., Asl, A., Bayazidi, Y., Mojahedian, M., and Davari, M. (2018). The Clinical Efficacy of Imiglucerase versus Eliglustat in Patients with Gaucher's Disease Type 1: A Systematic Review. J. Res. Pharm. Pract. *7*, 171.

Narain, Y., Wyttenbach, A., Rankin, J., Furlong, R.A., and Rubinsztein, D.C. (1999). A molecular investigation of true dominance in Huntington's disease. J. Med. Genet. *36*, 739–746.

Nguyen-Tran, D.H., Hait, N.C., Sperber, H., Qi, J., Fischer, K., Ieronimakis, N., Pantoja, M., Hays, A., Allegood, J., Reyes, M., et al. (2014). Molecular mechanism of sphingosine-1-phosphate action in Duchenne muscular dystrophy. DMM Dis. Model. Mech. *7*, 41–54.

Nucifora, J., Sasaki, M., Peters, M.F., Huang, H., Cooper, J.K., Yamada, M., Takahashi, H., Tsuji, S., Troncoso, J., Dawson, V.L., et al. (2001). Interference by huntingtin and atrophin-1 with cbp-mediated transcription leading to cellular toxicity. Science *291*, 2423–2428.

O'Sullivan, S., and Dev, K.K. (2017). Sphingosine-1-phosphate receptor therapies: Advances in clinical trials for CNS-related diseases. Neuropharmacology *113*, 597–607.

Parenti, G., Medina, D.L., and Ballabio, A. (2021). The rapidly evolving view of lysosomal storage diseases. EMBO Mol. Med. *13*.

Pirhaji, L., Milani, P., Leidl, M., Curran, T., Avila-Pacheco, J., Clish, C.B., White, F.M., Saghatelian, A., and Fraenkel, E. (2016). Revealing disease-associated pathways by network

integration of untargeted metabolomics. Nat. Methods *13*, 770–776.
Pirhaji, L., Milani, P., Dalin, S., Wassie, B.T., Dunn, D.E., Fenster, R.J., Avila-Pacheco, J., Greengard, P., Clish, C.B., Heiman, M., et al. (2017). Identifying therapeutic targets by combining transcriptional data with ordinal clinical measurements. Nat. Commun. *8*.
Reiner, A., Dragatsis, I., and Dietrich, P. (2011). Genetics and neuropathology of Huntington's disease. Int. Rev. Neurobiol. *98*, 325–372.
Riguet, N., Mahul-Mellier, A.L., Maharjan, N., Burtscher, J., Croisier, M., Knott, G., Hastings, J., Patin, A., Reiterer, V., Farhan, H., et al. (2021). Nuclear and cytoplasmic huntingtin inclusions exhibit distinct biochemical composition, interactome and ultrastructural properties. Nat. Commun. *12*.
Saftig, P., and Klumperman, J. (2009). Lysosome biogenesis and lysosomal membrane proteins: trafficking meets function. Nat. Rev. Mol. Cell Biol. *10*, 623–635.
Saudou, F., and Humbert, S. (2016). The Biology of Huntingtin. Neuron *89*, 910–926.
Sbodio, J.I., Snyder, S.H., and Paul, B.D. (2018). Golgi stress response reprograms cysteine metabolism to confer cytoprotection in Huntington's disease. Proc. Natl. Acad. Sci. U. S. A. *115*, 780–785.
Serra, M., and Saba, J.D. (2010). Sphingosine 1-phosphate lyase, a key regulator of sphingosine 1-phosphate signaling and function. Adv. Enzyme Regul. *50*, 349–362.
Singh, A., and Agrawal, N. (2021). Metabolism in Huntington's disease: a major contributor to pathology. Metab. Brain Dis.
Tabrizi, S.J., Flower, M.D., Ross, C.A., and Wild, E.J. (2020). Huntington disease: new insights into molecular pathogenesis and therapeutic opportunities. Nat. Rev. Neurol. *16*, 529–546.
Vollmuth, T.A. (2018). Caramel color safety - An update. Food Chem. Toxicol. *111*, 578–596.
Wanker, E.E., Ast, A., Schindler, F., Trepte, P., and Schnoegl, S. (2019). The pathobiology of perturbed mutant huntingtin protein-protein interactions in Huntington's disease. J. Neurochem. *151*, 507–519.
Wheeler, V.C., White, J.K., Gutekunst, C.A., Vrbanac, V., Weaver, M., Li, X.J., Li, S.H., Yi, H., Vonsattel, J.P., Gusella, J.F., et al. (2000). Long glutamine tracts cause nuclear localization of a novel form of huntingtin in medium spiny striatal neurons in HdhQ92 and HdhQ111 knock-in mice. Hum. Mol. Genet. *9*, 503–513.
Wilton, D.K., and Stevens, B. (2020). The contribution of glial cells to Huntington's disease pathogenesis. Neurobiol. Dis. *143*.
Won, S., Incontro, S., Nicoll, R.A., and Roche, K.W. (2016). PSD-95 stabilizes NMDA receptors by inducing the degradation of STEP61. Proc. Natl. Acad. Sci. U. S. A. *113*, E4736–E4744.

Yu, X.Q., Kramer, J., Moran, L., O'Neill, E., Nouraldeen, A., Oravecz, T., and Wilson, A.G.E. (2010). Pharmacokinetic/pharmacodynamic modelling of 2-acetyl-4(5)-tetrahydroxybutyl imidazole-induced peripheral lymphocyte sequestration through increasing lymphoid sphingosine 1-phosphate. Http://Dx.Doi.Org/10.3109/00498251003611376 *40*, 350–356.

Supplemental Information

Pharmacological targeting of Sphingosine-1-phosphate Lyase (SGPL1) modulates (glyco)sphingolipid metabolism and results therapeutically effective in experimental models of Huntington's disease

Giuseppe Pepe[1], Luca Capocci[1], Federico Marracino[1], Natalia Realini[2], Aynur Sönmez[3,11], Paola Lenzi[4], Katiuscia Martinello[1], Tiziana F Bovier[5,6], Terry Jo Bichell[7], Pamela Scarselli[1], Clotilde Di Cicco[1], Aaron Bowman[8], Filomena A Digilio[5], Sergio Fucile[1,9], Francesco Fornai[1,4], Andrea Armirotti[2], Rosanna Parlato[10], Alba Di Pardo[1] and Vittorio Maglione[1,12,*]

[1]IRCCS Neuromed; Pozzilli (IS), 86077, Italy

[2]Analytical Chemistry Lab, Fondazione Istituto Italiano di Tecnologia, Via Morego 30, 16163 Genoa, Italy

[3] Institute of Applied Physiology, Ulm University, Ulm, Germany.

[4]Department of Translational Research and New Technologies in Medicine and Surgery, University of Pisa, Via Roma 55, 56126 Pisa, Italy.

[5]Research Institute on Terrestrial Ecosystems (IRET), UOS Naples-CNR,
Via Pietro Castellino 111, 80131 Naples, Italy

[6] Department of Pediatrics Columbia University Vagelos College of Physicians and Surgeons, New York, NY, USA; Center for Host–Pathogen Interaction, Columbia University Vagelos College of Physicians and Surgeons, New York, NY, USA.

[7]Vanderbilt Brain Institute, Vanderbilt University, United States

[8]School of Health Sciences, Purdue University, West Lafayette, IN, United States of America.

[9]Department of Physiology and Pharmacology, Istituto Pasteur-Fondazione Cenci Bolognetti, University of Rome Sapienza, Rome, Italy.

[10]Division for Neurodegenerative Diseases, Department of Neurology, Mannheim Center for Translational Neuroscience, Medical Faculty Mannheim, Heidelberg University, Mannheim, Germany; Institute of Applied Physiology, Ulm University, Ulm, Germany

[11]Present address: RNA Molecular Biology, Fonds de la Recherche Scientifique (F.R.S./FNRS), Université Libre de Bruxelles (ULB), Biopark campus, Gosselies, Belgium.

[12]Lead contact

[*]Correspondence: vittorio.maglione@neuromed.it (V.M.)

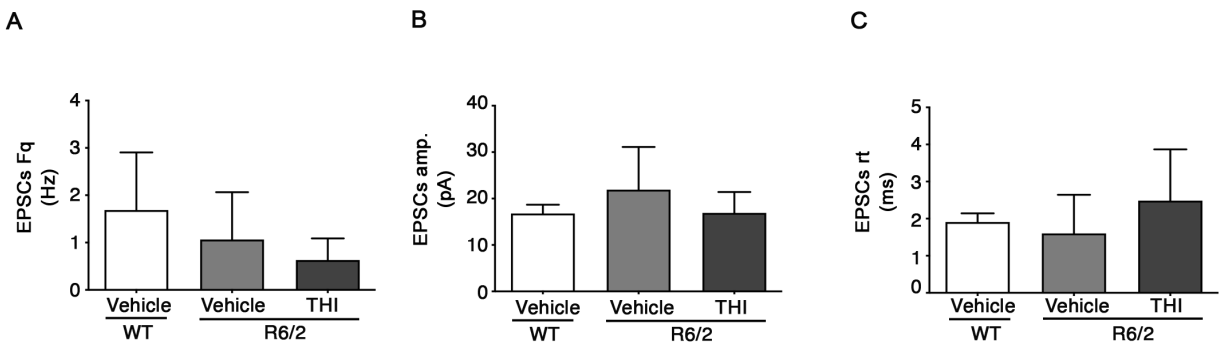

Figure S1, Related to Figure 2. THI treatment preservers white-matter integrity and ameliorates synaptic activity in HD cortical pyramidal neurons

(A) Bar graphs representing mean values of EPSC frequency obtained from 5, 5 and 7 cells from vehicle-treated WT, Vehicle- and THI-Treated R6/2 mice, respectively.

(B) Bar graphs representing mean of EPSC amplitude obtained from 5, 5 and 7 cells from vehicle-treated WT, vehicle- and THI-Treated R6/2 mice, respectively.

(C) Bar graphs representing mean of EPSC rise-time$_{10\text{-}90}$ obtained from 5, 5 and 7 cells from vehicle-treated WT, Vehicle- and THI-Treated R6/2 mice, respectively.

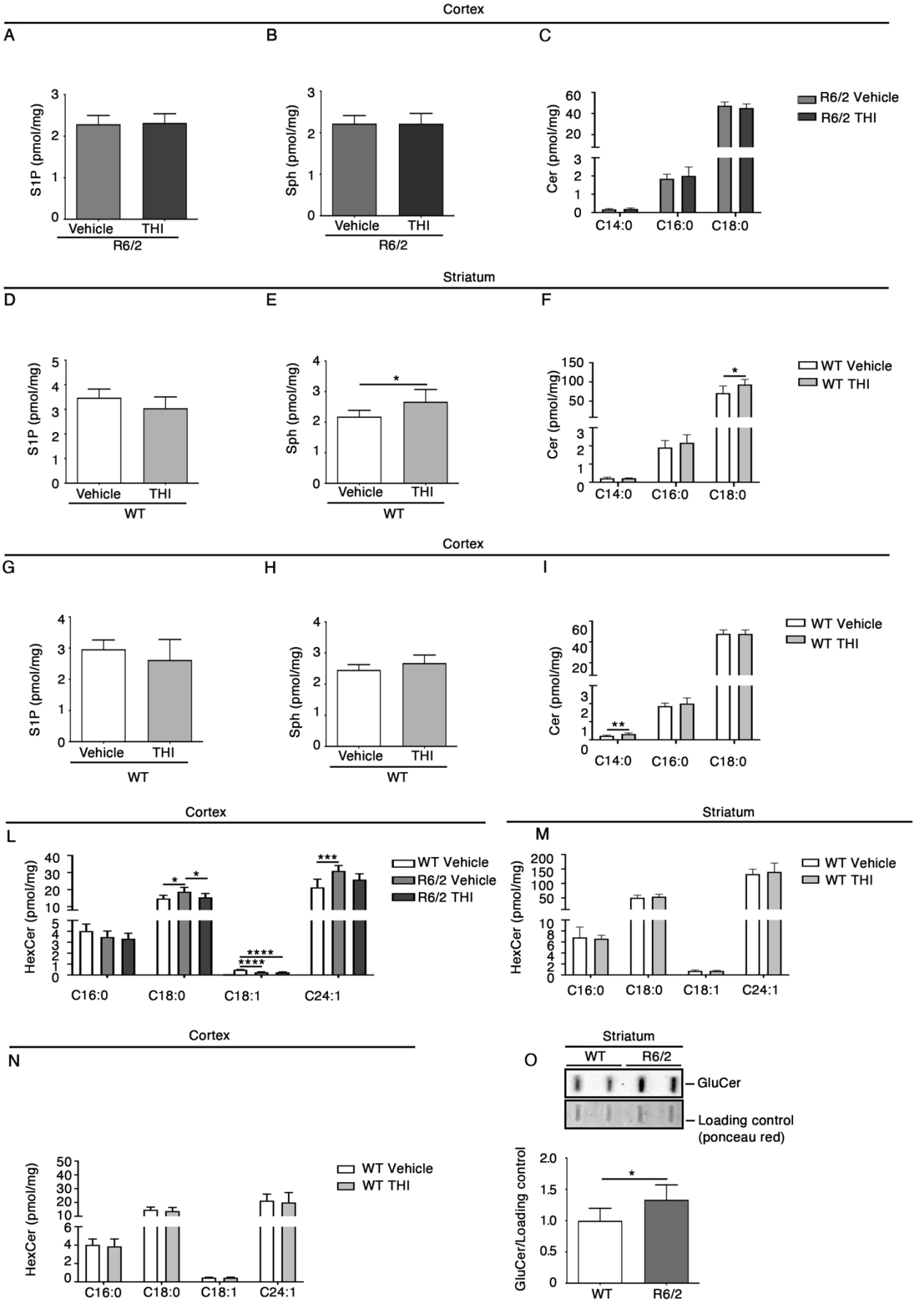
Cortex
A
S1P (pmol/mg)
Vehicle
THI
R6/2
B
Sph (pmol/mg)
Vehicle
THI
R6/2
C
Cer (pmol/mg)
C14:0
C16:0
C18:0
R6/2 Vehicle
R6/2 THI
Striatum
D
S1P (pmol/mg)
Vehicle
THI
WT
E
Sph (pmol/mg)
*
Vehicle
THI
WT
F
Cer (pmol/mg)
*
C14:0
C16:0
C18:0
WT Vehicle
WT THI
Cortex
G
S1P (pmol/mg)
Vehicle
THI
WT
H
Sph (pmol/mg)
Vehicle
THI
WT
I
Cer (pmol/mg)
**
C14:0
C16:0
C18:0
WT Vehicle
WT THI
Cortex
L
HexCer (pmol/mg)
*
*
****
****
***
C16:0
C18:0
C18:1
C24:1
WT Vehicle
R6/2 Vehicle
R6/2 THI
Striatum
M
HexCer (pmol/mg)
C16:0
C18:0
C18:1
C24:1
WT Vehicle
WT THI
Cortex
N
HexCer (pmol/mg)
C16:0
C18:0
C18:1
C24:1
WT Vehicle
WT THI
Striatum
O
WT
R6/2
GluCer
Loading control
(ponceau red)
GluCer/Loading control
*
WT
R6/2

Figure S2, Related to Figure 4. THI treatment modulates the expression of sphingolipid metabolizing enzymes and restores normal levels of hexosylceramides in HD mice

(A) Lipidomic analysis by LC-MS/MS of S1P in cortical tissues of vehicle- and THI-treated R6/2 mice at 11 weeks of age. Values are represented as mean ± SD. N = 7 for each group of mice.

(B) Lipidomic analysis by LC-MS/MS of Sph in cortical tissues of vehicle- and THI-treated R6/2 mice at 11 weeks of age. Values are represented as mean ± SD. N = 7 for each group of mice.

(C) Lipidomic analysis by LC-MS/MS of Cer in cortical tissues of vehicle- and THI-treated R6/2 mice at 11 weeks of age. Values are represented as mean ± SD. N = 7 for each group of mice.

(D) Lipidomic analysis by LC-MS/MS of S1P in striatal tissues of vehicle- and THI-treated WT mice at 11 weeks of age. Values are represented as mean ± SD. N = 7 for vehicle-treated WT mice, N=5 for THI-treated WT mice.

(E) Lipidomic analysis by LC-MS/MS of Sph in striatal tissues of vehicle- and THI-treated WT mice at 11 weeks of age. Values are represented as mean ± SD. N = 7 for vehicle-treated WT mice, N=5 for THI-treated WT mice.

(F) Lipidomic analysis by LC-MS/MS of Cer in striatal tissues of vehicle- and THI-treated WT mice at 11 weeks of age. Values are represented as mean ± SD. N = 7 for vehicle-treated WT mice, N=5 for THI-treated WT mice.

(G) Lipidomic analysis by LC-MS/MS of S1P in cortical tissues of vehicle- and THI-treated WT mice at 11 weeks of age. Values are represented as mean ± SD. N = 7 for vehicle-treated WT mice, N=5 for THI-treated WT mice.

(H) Lipidomic analysis by LC-MS/MS of Sph in cortical tissues of vehicle- and THI-treated WT mice at 11 weeks of age. Values are represented as mean ± SD. N = 7 for vehicle-treated WT mice, N=5 for THI-treated WT mice.

(I) Lipidomic analysis by LC-MS/MS of Cer in cortical tissues of vehicle- and THI-treated WT mice at 11 weeks of age. Values are represented as mean ± SD. N = 7 for vehicle-treated WT mice, N=5 for THI-treated WT mice.

(L) Lipidomic analysis by LC-MS/MS of HexCer 16:0, 18:0, 18:1 and 24:1 in cortical tissues of vehicle-treated WT and vehicle- and THI-treated R6/2 mice at 11weeks of age. Values are represented as mean ± SD. N = 7 for each group of mice. One-Way ANOVA, *$p < 0.05$; ***, $p < 0.001$; ****, $p < 0.0001$.

(M) Lipidomic analysis by LC-MS/MS of HexCer 16:0, 18:0, 18:1 and 24:1 in striatal tissues of vehicle and THI-treated WT mice at 11weeks of age. Values are represented as mean ± SD. N = 7 for vehicle-treated WT mice, N=5 for THI-treated WT mice.

(N) Lipidomic analysis by LC-MS/MS of HexCer 16:0, 18:0, 18:1 and 24:1 in cortical tissues of vehicle- and THI-treated WT mice at 11weeks of age. Values are represented as mean ± SD. N = 7 for vehicle-treated WT mice, N=5 for THI-treated WT mice.

(O) Slot-Blotting and densitometric analysis of GluCer in striatal tissues from WT and R6/2 mice at 11 weeks of age. Values are represented as mean ± SD. N = 5 for each group of mice. Ponceau red was used as total protein loading control. Un-paired *t*-test, *$p < 0.05$.

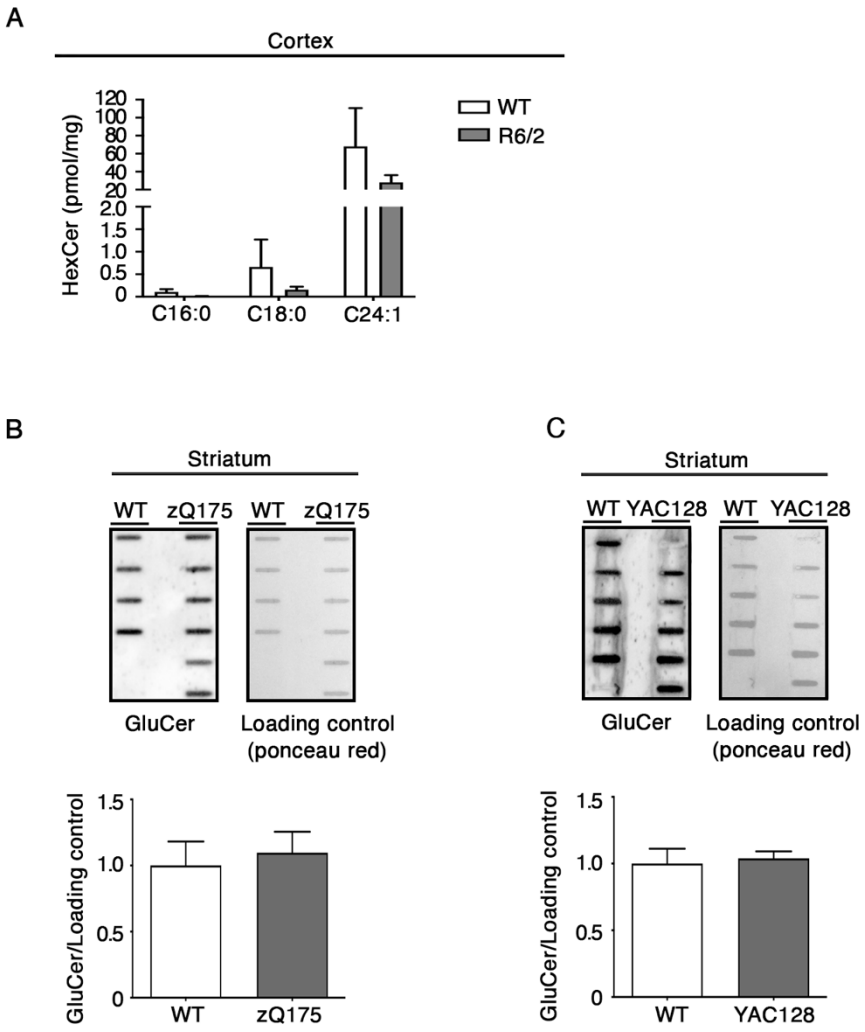

Figure S3, Related to Figure 5. Defects in HexCer metabolism are detectable early in the disease course in different HD mouse models

(A) Lipidomic analysis by LC-MS/MS of HexCer 16:0, 18:0 and 24:1 in cortical tissues of pre-manifest (4-week-old) R6/2 mice and aged-matched WT littermates. Values are represented as mean ± SD. N = 4 for each group of mice.

(B) Slot-Blotting and densitometric analysis of GluCer in striatal tissues from WT and heterozygous zQ175 mice at 20 weeks of age. Values are represented as mean ± SD. N = 4 for WT mice; N = 6 for HD mice. Ponceau red was used as total protein loading control.

(C) Slot-Blotting and densitometric analysis of GluCer in striatal tissues from WT and YAC128 mice at 13 weeks of age. Values are represented as mean ± SD. N = 5 for each group of mice. Ponceau red was used as total protein loading control.